TECTONICS, VOL. 12, NO. 5, PAGES 1140-1169, OCTOBER 1993

TECTONIC ROLE OF ACTIVE FAULTING IN CENTRAL OREGON

Silvio K. Pezzopane,[1] and Ray J. Weldon II
Department of Geological Sciences, University of Oregon, Eugene

Abstract. Geologic and geodetic studies in California indicate that about 1 cm yr^{-1} of right-lateral shear occurs across what has been referred to as the Eastern California Shear Zone. Northwest trending zones of dextral, sinistral, and normal faults splay eastward from the San Andreas system, continuing through the Mojave Desert, east of the Sierra Nevada, and northward along the Central Nevada and Walker Lane fault zones. Aerial photography, field investigations, and fault studies in southern and central Oregon, compiled with a comprehensive analysis of previous studies nearby, indicate that latest Pleistocene and Holocene fault activity is concentrated along four zones that stretch northward into the Cascade volcanic arc and across the northwestern edge of the Basin and Range Province. The Oregon zones appear to continue the activity in eastern California and northwestern Nevada northward and provide a connection to seismically active zones in southern and central Washington. Several techniques are applied to fault data from the Oregon zones in an attempt to estimate the overall direction and rate of motion across them. The orientations and styles of faults younger than middle Tertiary are used with models of oblique rifting to estimate that the motion of western Oregon is ~N60° ± 20°W, relative to North America. Summation of geologic moment tensors from faults with latest Pleistocene and Holocene slip yields a direction ~N90°± 30°W at a rate of ~0.5 mm yr^{-1}. This result is a minimum since many fault scarps have not been preserved or recognized, and additional deformation is recorded as folding and tilting. Crustal strain associated with slip during 76 of the largest crustal earthquakes in the past 120 years located along this broad zone from northern California and Nevada, across Oregon, to Washington and Vancouver Island, indicates motions at rates of 3 ± 1 mm yr^{-1} in a direction N55°± 10°W. Although the motion across central Oregon is much slower, its similarity in style with regions to the north and south suggests that the regional averages are meaningful. Oregon fault zones, taken together, may accommodate as much as 6 mm yr^{-1} oriented ~N60° to 70°W. A tectonic model of fault activity reveals that this proposed shear zone through Nevada, Oregon, and Washington can account for 10% to 20% of the total Pacific-North American transform motion and much of the lateral component of relative motion between the Juan de Fuca and North American plates.

INTRODUCTION

Oregon is surrounded by zones of active faults that have produced large-magnitude earthquakes; yet to date, few Holocene faults have been described in Oregon, and even fewer large magnitude earthquakes have been recorded here. The Cascadia subduction zone lies off the west coast of Oregon and Washington and forms the convergent boundary between the Juan de Fuca and North American plates (Figure 1). The Cascadia interface is thought to accommodate relative motion of the Juan de Fuca plate beneath the coast at a rate of 40 to 45 mm yr^{-1} in a direction about N60°E [e.g., Riddihough, 1984; Nishimura et al., 1984; DeMets et al., 1990]. Inboard of the Cascadia boundary, the neotectonic regime changes from compression on the coast [e.g., Kelsey et al., 1992] to extension in the volcanic arc and Basin and Range Province [e.g., Smith, 1978; Taylor, 1990; Ludwin et al., 1991]. Although much is known about active faulting and deformation in California and Nevada, few young fault zones in Oregon have been studied to determine the styles and slip rates.

This study uses aerial photography to identify faults that appear to offset or deform young deposits in Oregon. Ensuing field investigations commonly reveal that faults displace late Pleistocene and Holocene lacustrine, alluvial, and colluvial deposits and locally cut late Pleistocene volcanic and pyroclastic units. Aerial photo interpretations and local field investigations are combined with published fault studies in an effort to recognize throughgoing zones of fault activity (Figure 2). In general, late Quaternary and Holocene faulting concentrates along four zones that traverse northward across central and eastern Oregon. These backarc and intraarc zones appear to be the northern continuation of a broad belt of historic seismicity and faulting that stretches from the San Andreas fault system in southern California, through the Mojave Desert and east of the Sierra Nevada, to northeastern California and central Nevada [e.g., Wallace, 1984] (Figures 1 and 2).

For many years, workers in California and Nevada have recognized that major zones of extension and dextral shear lie east of the Sierra Nevada, along the western edge of the Basin and Range Province [e.g., Wise, 1963; Shawe, 1965] (summarized by Stewart et al. [1968]). The kinematic connection of right-lateral and extensional faulting in the Basin and Range with Pacific-North America transform shear and the San Andreas fault system was recognized more than 20 years ago [Atwater, 1970]. However, only recently has the entire zone been studied in sufficient detail to assess its contribution to the total Pacific-North American plate motion.

Dokka and Travis [1990] define the "Eastern California shear zone" as a belt of faults that extend through the Mojave Desert and connect with right-lateral and normal faults east of the Sierra Nevada (Figure 1). A regional zone of dextral shear diverges from the San Andreas fault system in the Eastern Transverse Ranges, south of the Mojave Desert [Powell, 1981, 1993; Humphreys and Weldon, 1991; Powell and Weldon, 1992; Richard, 1992; Weldon et al., 1993]. Geologic and geodetic data in the Mojave Desert indicate a rate of 5 to more than 8 mm yr^{-1} of regional dextral shear that has been active since middle Miocene time [Dibblee, 1967; Powell, 1981, 1993; Dokka, 1983; Sauber et al., 1986; Dokka and Travis, 1990; Sauber, 1990; Savage et al., 1990; Powell and Weldon, 1992; Richard, 1992]. East of the Sierra Nevada and north of the Mojave, there are three major northwest trending right-lateral fault zones: the Death Valley-Furnace Creek, Hunter Mountain-Panamint Valley, and Owens Valley (Figure 1). Each zone shows an average late Quaternary slip rate of 1 to 3 mm yr^{-1} [Wernicke et al., 1989; Burchfiel et al., 1987; Lubetkin and Clark, 1988; Zhang et al., 1990], which together add up to the rate of deformation crossing the Mojave Desert.

[1] Now at U.S. Geological Survey, Denver Federal Center, Denver, CO 80225.

Paper number 92TC02950.
0278-7407/93/92TC-02950$10.00

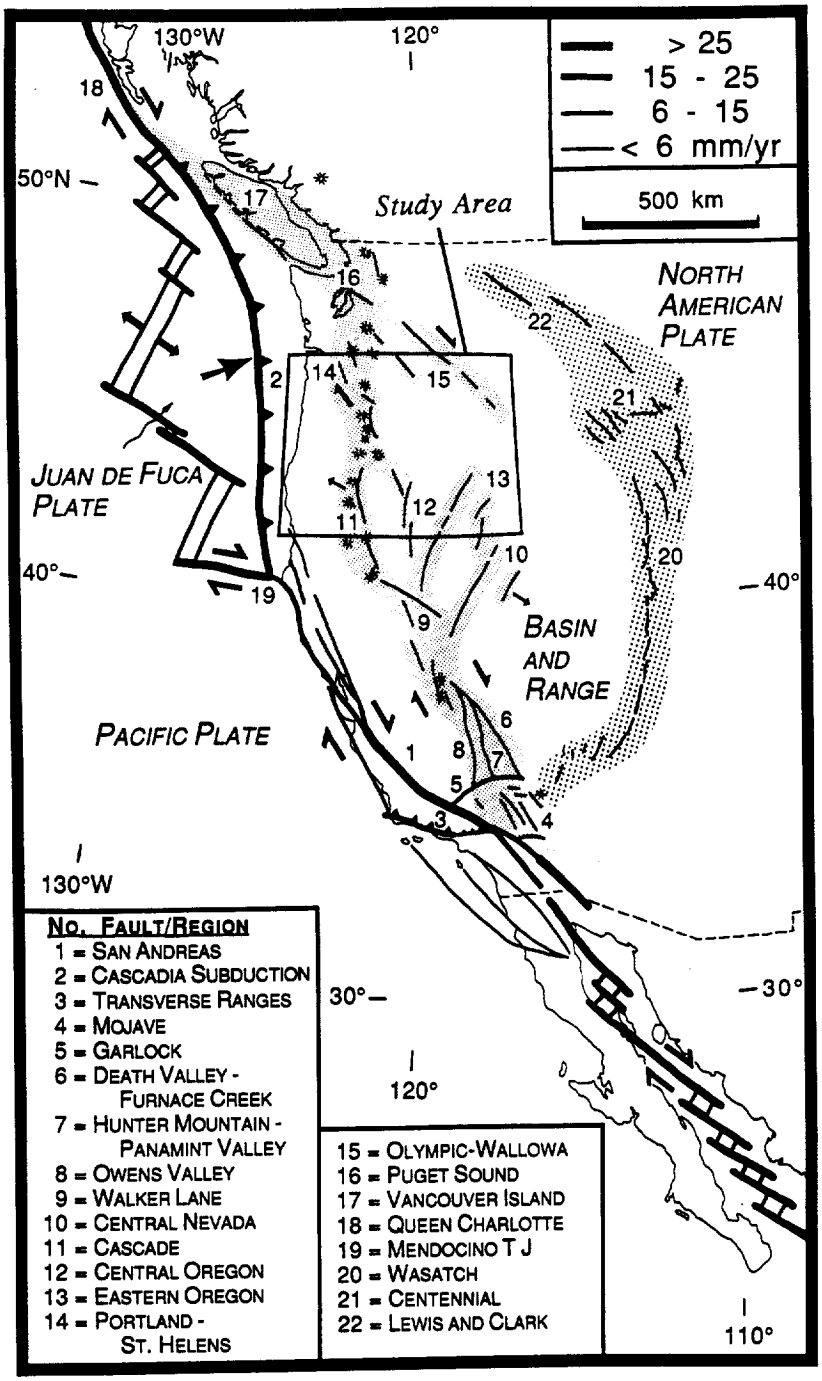

Fig. 1. Map of Pacific, North America, and Juan de Fuca plate boundaries, and recognized active fault zones idealized with line thickness proportional to fault zone slip rate (in mm yr^{-1}). Fault activity (labeled by number and stippled) is compiled from sources mentioned in the text. Dense stipple indicates the "eastern shear zone." Vent pattern shows Cascade volcanoes. Base map from Moore [1982].

A pulse of large earthquakes during the past 120 years ruptured faults in the Mojave Desert, Owens Valley, the Sierra Nevada frontal faults, and northward into the central Nevada seismic belt [Wallace, 1984], demonstrating that the zone is still active.

In west-central Nevada, the Holocene fault activity splits into the central Nevada seismic belt and the northern Walker Lane fault zone (Figures 1 and 2). Activity in the Walker Lane zone is recognized along northwest trending right-slip faults including the Pyramid Lake, Warm Springs Valley, Honey Lake, and Eagle Lake fault zones [e.g., Bell, 1984] (Figure 2). This zone has been active since Miocene time and forms the boundary between the Sierra Nevada and the Basin and Range Province [Shawe, 1965; Bell and Slemmons, 1982a; Wagner et al., 1989]. The Honey Lake, Pyramid Lake, and Eagle Lake fault zones each have average late Quaternary

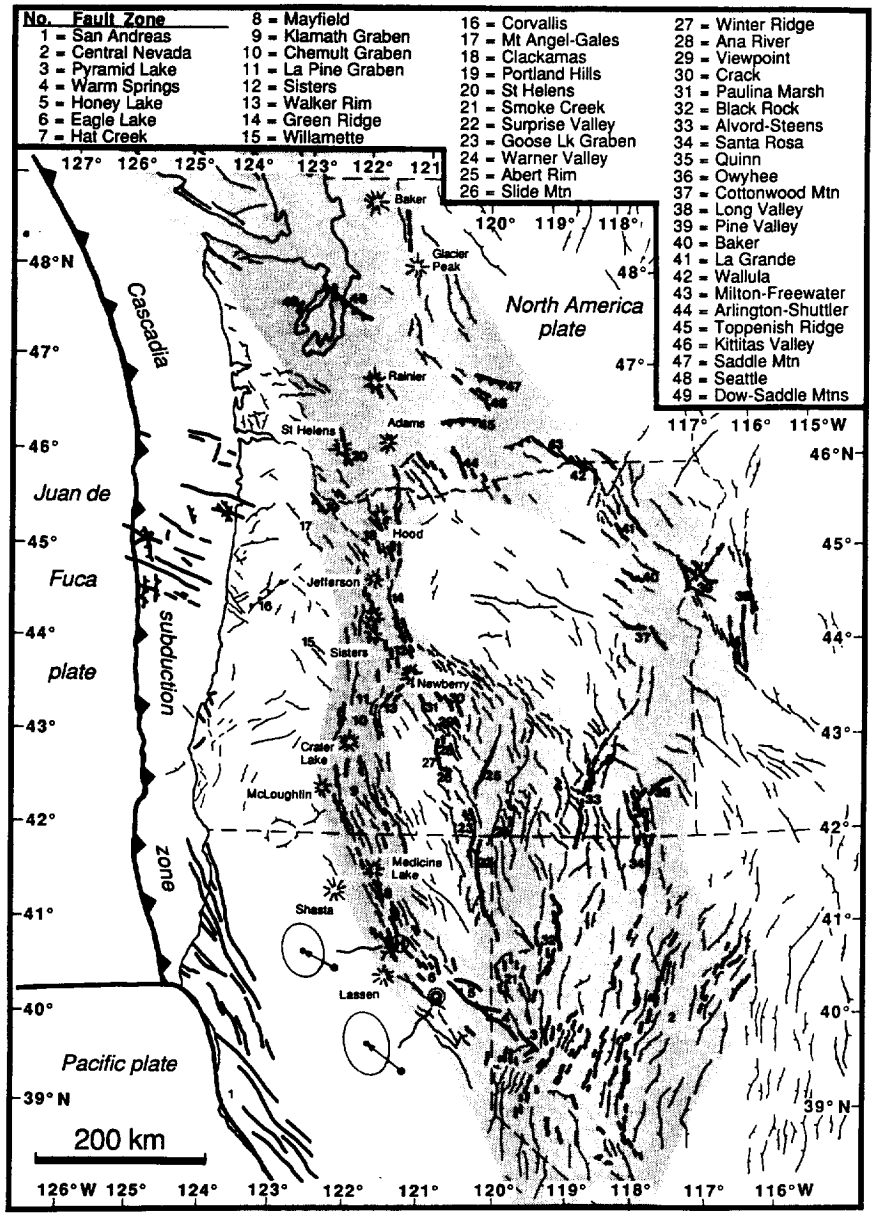

Fig. 2. Map of middle Tertiary and younger faults in the Pacific Northwest and northern California and Nevada. Late Quaternary and Holocene fault activity (bold lines) indicates active backarc and intraarc fault zones that stretch from northern California to southern Canada. Major, throughgoing zones of deformation are stippled; individual fault zones are numbered. Vent pattern shows Cascade volcanoes. Circled H and Q in northern California show the very long baseline interferometry (VLBI) stations HATC and QUIN connected to a vector indicating the rate of change of station positions and 95% confidence error ellipses [from Sauber, 1990]. The motions are relative to fixed North America, which includes a station at Ely, Nevada (ELY; not shown, but near lower right corner of Figure 2). The vector velocities at HATC (9.4 ± 2.6 mm yr^{-1}, N62°W ± 8°) and QUIN (12.0 ± 3.1 mm yr^{-1}, N52°W ± 9°) indicate that as much as 1 cm yr^{-1} of crustal strain is concentrated along this zone. Base map from Walker and MacLeod [1991], Jennings [1992], Stewart and Carlson [1978], Bond and Wood [1978], Walsh et al. [1987], modified with information from Smith and Lindh [1978], Nakata et al. [1982], U.S. Army Corps of Engineers [1983a], McInelly and Kelsey [1990], Goldfinger et al. [1992b], Pezzopane [1993], and those mentioned in text.

slip rates as much as 2 mm yr^{-1} [Wills and Borcherdt, 1990; Bell and Slemmons, 1982a; Roberts and Grose, 1982].

Regional geodetic studies and kinematic models of the western plate boundary of North America place only about two thirds of the total Pacific-North American plate motion on the San Andreas fault system [e.g., Minster and Jordan, 1984, 1987; Weldon and Humphreys, 1986; DeMets et al., 1987, 1990; Sauber, 1990; Ward, 1990; Argus and Gordon, 1991]. These models commonly place the remainder on faults east of the Sierra Nevada, in the Basin and Range Province. Very long baseline interferometry (VLBI) stations west of the Walker Lane fault zone (Figure 1) record the direction and rate of relative motion between the northern end of the Sierra Nevada block and North America. Relative to "fixed" stations at Ely, (ELY) Nevada and farther east, the stations at Hat Creek (HATC) and Quincy (QUIN), California, are moving in a direction N35° to 65°W, at a rate of 8 to 12 mm yr^{-1} (Figure 2), depending upon various inversion techniques [e.g., Clark et al., 1987; Sauber, 1990; Ward, 1990; Argus and Gordon, 1991]. These VLBI results provide a useful basis of comparison for this study.

North of Oregon, diffuse zones of crustal seismicity and late Quaternary faulting stretch across southern Washington and into Puget Sound (Figures 1 and 2). Seismicity studies indicate that right-slip and extensional faulting occurs in the Portland Basin [e.g., Yelin and Patton, 1991] and in the Cascade arc near Mount St. Helens [e.g., Weaver et al., 1987], whereas geological and seismological evidence indicates that right-slip and thrust faulting occurs in southeastern Washington and Puget Sound [e.g., Yount and Holmes, 1992; Campbell and Bentley, 1981; Ludwin et al., 1991]. Active faults in Washington occur mainly along the Olympic-Wallowa trend (Figure 2) and appear to connect with recognized zones of faulting in northern Oregon. We propose that the kinematic links between seismic zones inboard of the plate boundary in Washington and those of the Eastern California Shear Zone are the active fault zones in Oregon.

This study attempts to demonstrate that the Oregon fault zones are active, to quantify the direction and rate of motion across the zones, and to relate this deformation to relative motion across the plate boundary at the coast. We hypothesize that these "inboard" fault zones separate a relatively stable slice of continental lithosphere from North America, moving it northwestward, possibly rotating it, and significantly changing the relative motion across the Cascadia plate boundary farther to the west.

Three approaches allow us to test this hypothesis. The orientations and styles of middle Tertiary and younger faulting in central Oregon are used with models of oblique rifting to estimate the direction of combined extension and shear. The orientations and displacements of mapped late Quaternary and Holocene faults are used to estimate geological moment tensors. The moment tensors are summed, and the components of crustal strain are calculated with methods developed by Brune [1968], Kostrov [1974], and Jackson and McKenzie [1988]. These approaches allow us to infer the overall motion across a zone that consists of a diverse group of structures. The analysis includes summing the seismic moments and calculating the strain associated with slip during 76 of the largest crustal earthquakes which occurred in the past 120 years in the area from the Basin and Range Province of northern California and Nevada, across Oregon, to Washington and Vancouver Island where this "eastern zone" appears to reconnect to the plate boundary. The velocities of the plates bounding the fault zones are determined from the strain tensors and are synthesized into a kinematic model. The kinematic model integrates the outcome of this analysis with the results of regional geodetic and plate motion studies. After a brief examination of middle Tertiary and Holocene fault patterns in central Oregon, and presentation of the active fault data and seismicity analyses, results of the study are discussed in relation to current understanding of the relative motion between the North America, Juan de Fuca, and Pacific plates in the vicinity of Oregon.

FAULT ORIENTATIONS AND OBLIQUE RIFTING OF CENTRAL OREGON

Faults in central Oregon are similar to those in northeastern California and western Nevada and can be divided into two common orientations, one striking northwest and the other N-NE (Figures 2 and 3). In Oregon, the northwest set of faults is dominant in number, and many of the faults in it are parallel or subparallel over longer distances than are those in the N-NE set. However, the faults striking N-NE are the major range-bounding faults which show the greatest normal displacement. Although these faults do not occur in long, parallel rows like the northwest set, they combine to form chains of deep grabens separated by horsts that trend N-NE.

Although the major structural features in southern Oregon are familiar to many geologists, there has been some debate about the actual kinematics of fault displacement. Pease [1969] and Lawrence [1976], among others, suggest the northwest trending faults are major right-lateral structures that control the orientation and offset of the N-NE-trending range-bounding normal faults. On the other hand, Donath [1962] recognizes both right-lateral and left-lateral displacements on faults in the study area, and is widely cited as evidence for orthorhombic symmetry of normal faulting [e.g., Reches, 1983], rather than the standard bilateral symmetry seen elsewhere in the Basin and Range and predicted by Anderson-Coulomb theory of faulting. In contrast, Hamilton and Myers [1966] explain the fault pattern to result from both right-lateral shear and extension. Likewise, Stewart et al. [1975] interpret a belt of young faults, extending from central Oregon to central Nevada, to represent a deep-seated zone of both right-lateral shear and tensional movement.

Knowledge of the extension direction gives a nonunique kinematic constraint on the initial structural configuration and can help test different kinematic solutions. Often, one can infer possible kinematic solutions from a population of structures by comparison with fault patterns from experimental models. To constrain better the directions of horizontal strain and extension, Withjack and Jamison [1986] developed analytical and experimental models to simulate deformation produced by rifting. They show that extension and shear both contribute to oblique rifting, and that the relative amounts of extension and shear depend upon the acute angle (α) between the rift trend (R) and the relative displacement direction between opposite sides of the rift (Figure 3). Generally if α is much less than 30°, either strike-slip faults or conjugate sets of oblique-slip faults form in the rift (Figure 3). And if α exceeds 30°, normal faults form parallel to the rift. In particular, strike-slip, oblique-slip, and normal faults all form if α is near 30°. With $\alpha \approx 30°$ and right-lateral shear across the rift, sinistral and dextral strike-slip faults trend subparallel and at

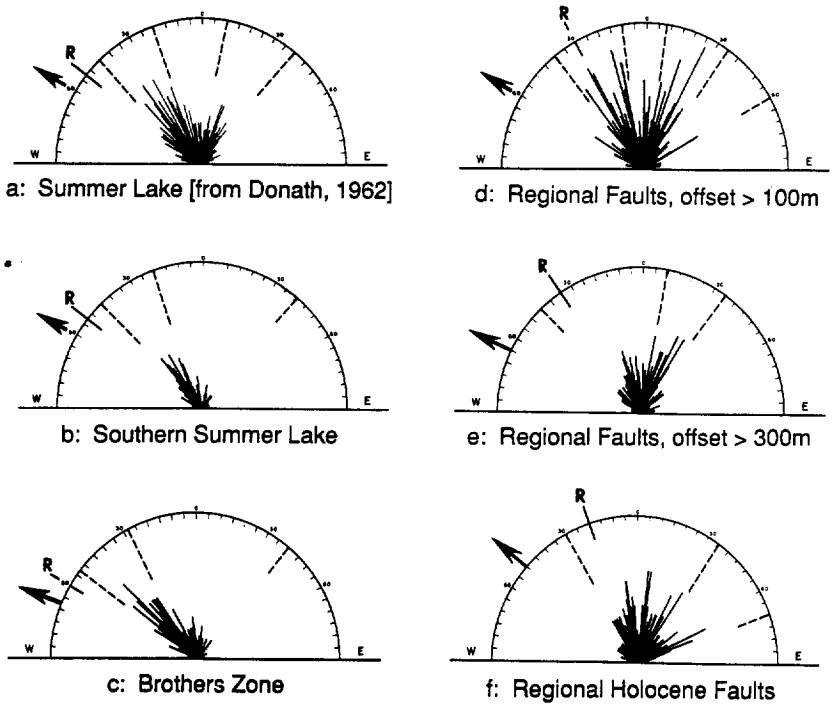

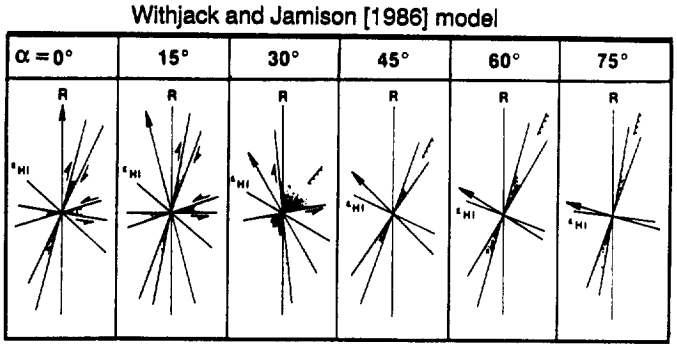

Fig. 3. Fault-strike frequency diagrams and the Withjack and Jamison [1986] model of oblique rifting. (Top) Strikes of each fault or fault segment at least 1 km in length, taken from areas along the Central and Eastern Oregon fault zones (shown in Figure 6). Strikes are plotted at 1° intervals, and the radius of each diagram equals 18 fault segments. The predominant fault orientations (grouped with five dashes) and the overall range of the broader distribution (including faults out to three dashes) are modeled with the Withjack and Jamison approach. Fault strikes from (a) the Summer Lake area, 625 fault segments about 1 km in length, from Donath [1962]; (b) south of the Summer Lake area, 198 fault segments about 5 km in length; (c) the Brothers fault zone, 296 fault segments over 1 km in length; (d) faults with offsets greater than 100 m in the entire region shown in Figure 6, 489 fault segments, 1 km in length; (e) faults with offsets greater than 300 m in the entire region, 361 fault segments, 1 km in length; (f) active faults in the region, 464 fault segments (listed in Table 1), 1 km in length (bold in Figure 6). Most of the faults, including those with smaller offsets, strike northwest; whereas the horst and graben faults with the most offset strike north to northeast. (Bottom) Withjack and Jamison [1986] model of oblique rifting showing fault patterns associated with combined dextral shear and extension. The geometries of faulting and directions of maximum horizontal extension (ε_{H1}) are given for different values of α, the acute angle between the overall direction of rifting (arrow) and the strike of the rift (R). Applying this model to faults in central Oregon and the northwestern Basin and Range Province indicates that α is between 0° and 30° from the rift and that the faults, taken together, accommodate motion of western Oregon in a direction N40° to 80°W (arrows) relative to North America.

large angles to the rift trend, respectively. Normal and normal-oblique faults range in strike somewhere between these extremes, averaging about 30° clockwise from the rift trend.

To determine the style of faulting with the Withjack and Jamison [1986] model, topographic and geologic maps [Walker and MacLeod, 1991; Stewart and Carlson, 1978] were used to tabulate fault strikes in central Oregon (Figure 3). Faults were divided into one-kilometer segments and the average strike and offset for each segment was recorded. We sampled faults that are mapped just south of Summer Lake (Figure 3b) and along the Brothers fault zone (Figure 3c), which are areas near an earlier study by Donath [1962], as well as across larger regions nearby (Figures 3d and 3e).

In earlier studies, Donath [1962] found that Late Tertiary fault strikes in the Summer Lake area of central Oregon (Figure 3a) can be divided into two dominant trends which average about N35° ± 15°W and N25° ± 15°E (average strikes lie between orientations indicated with five dashes, Figure 3). At places, the northwest and the N-NE sets of faults both show repeated Quaternary displacements that are predominantly normal, although evidence exists for small components of left- or right-slip on individual faults [e.g., Donath, 1962] (this study). Generally, this pattern is consistent with most of the Late Tertiary and younger faults in central Oregon, which strike over a broad range from N70°W to N70°E and exhibit predominantly normal and normal-oblique slip (Figure 3).

Application of the Withjack and Jamison [1986] model to fault strikes along the central Oregon zone indicates that $\alpha \leq 30°$ is compatible with the wide range, and in some cases, distinct sets of fault orientations. For example, the two fault orientations at Summer Lake (Figure 3a) fit the model best with α nearer 0° to 15°, rather than a larger value (i.e., $\alpha > 45°$), which predicts a single and much narrower range of fault strikes. Matching the model geometry with the Oregon fault orientations predicts that the direction of oblique rifting near Summer Lake is ~N60°W. The inferred rift (R) trends ~N50°W, and maximum extensional strain (ε_{H1}) is oriented ~E-W.

Nearby regions of Summer Lake and the Brothers zone are characterized by predominantly northwest striking faults (~N35° ± 15°W, between orientations indicated with five dashes, Figure 3b and 3c). Compared with faults along the central Oregon zone, those along the Brothers zone, where the recognized style of slip is dominantly right-lateral [e.g., Lawrence, 1976], are consistent with $\alpha \leq 15°$ and oblique rifting slightly more westward (N60° to 75°W). The N-NE fault set recognized by Donath is apparent but less defined (orientations to three dashes, Figure 3b and 3c). The overall strike distribution (from ~N50°E to N40°W, i.e., three dashes in Figures 3b and 3c) can also be fit with $\alpha \approx 30°$. In this case ($\alpha \approx 30°$ is not shown in Figure 3b or 3c), the Withjack and Jamison model predicts that the direction of rifting does not change considerably (~N60°W), whereas the maximum extensional strain (ε_{H1}) is oriented ~N80°W and the rift (R) is oriented ~N30° to 40°W.

Throughout southeastern Oregon and northwestern Nevada the faults that show the largest vertical separations mostly strike N-NE (Figure 3d and 3e). A broad range of strikes is apparent, perhaps consistent with α roughly 30° and oblique rifting ~N60°W. Though the larger northeast striking normal faults appear to accommodate more crustal strain, the northwest striking faults are relatively more numerous and may provide a means of transferring slip across the larger horsts and grabens. Under such conditions, the northwest fault set accommodates mainly dextral slip, and the N-NE set accommodates normal to left-oblique slip. Together, the fault sets serve to accommodate overall oblique motion in a direction N50° to 70°W. This pull-apart pattern of large extensional basins located between oblique-slip fault zones has been recognized throughout the world [e.g., Withjack and Jamison, 1986; Aydin and Schultz, 1990; Chorowicz and Sorlien, 1992; Ring et al., 1992]. However, in this part of the western Basin and Range Province, the northwest striking oblique-slip faults are broadly distributed and do not appear to show a clear stepover geometry as they do to the south, for example along faults of the Eastern California shear zone [e.g., Dokka and Travis, 1990; Wernicke et al., 1988; Burchfiel et al., 1987]. This may be a consequence of relatively less slip in Oregon or the response of the extensive Tertiary basalt cover.

The late Tertiary fault pattern along the central Oregon zone closely resembles that predicted by the Withjack and Jamison [1986] model of oblique rifting, with α less than or equal to 30°, right-oblique shear, and overall motion across this zone in a direction N50° to 70°W. If the northwest faults accommodate largely normal motion, then the overall motion across the region is more westerly. However, if northwest faults accommodate mostly right-lateral slip, then the rifting direction is more northwestward. It will be useful to apply this model of oblique rifting to a more-regional data set of younger, active faults, and to compare the results with those derived from the older faults.

ACTIVE FAULT ZONES IN OREGON

Interpretations of aerial photography, field investigations, and a systematic review of published information, reveals evidence for late Pleistocene and Holocene fault activity that is concentrated along four zones which cross Oregon roughly from north to south (Figure 2). The Cascade zone can be traced from Mount Lassen to Mount St. Helens and consists of normal faults that bound the High Cascade graben and right-slip faults that traverse the arc. Left-stepping normal and normal-oblique faults define the Central Oregon zone which merges with the Cascade zone near Newberry volcano. Two eastern Oregon zones (Figure 2) traverse northeastward across northwestern Nevada into southeastern Oregon. The westernmost Eastern Oregon zone may connect with the intraarc zone via the Brothers fault zone, or both Eastern Oregon zones may connect to northwest striking right-slip faults in northeastern Oregon and southern Washington. Activity along each of these zones will be described in the order that they are located along the zone in a direction from south to north.

Cascade Zone

The Cascade fault zone consists of normal faults and right-slip shear zones located along the southern Cascade arc from Mount Lassen to Mount St. Helens (Figure 2). The broad region of distributed faulting and volcanism at the northern end of the Walker Lane pinches and merges northward into the Cascades in the region between Mount Lassen and Crater Lake [Grose et al., 1989]. Between Lassen Peak and Medicine Lake volcano, several left-stepping Holocene fault zones show average slip rates of ~1 mm yr^{-1} and evidence for small components of right-slip [e.g., Wills, 1991], including the Hat

Creek fault [Muffler and Clynne, 1989; Wills, 1991] and the Mayfield fault [e.g., Wills, 1991]. Pleistocene and younger strata are offset by faults in the Klamath, Chemult, and La Pine grabens, which can account for 5 to 10% extension and show as much as 2 km of Quaternary structural relief [Sherrod and Pickthorn, 1989]. These structures are similar to other intraarc faults along the zone and are consistent with average slip rates of ~1/2 to 1 mm yr^{-1}. Additional extension may be associated with crustal growth from volcanic infilling of fissures and vents such as at Mount Lassen [Guffanti et al., 1990], Medicine Lake [Donnelly et al., 1990], and other volcanic centers within the arc.

Northwest striking right-slip faults traverse the axis of the arc and appear to alternate with zones of extension. For example, the Sisters fault zone (Figure 2) strikes northwest toward the Three Sisters volcanoes and is composed of en echelon zones of contemporaneous late Quaternary and Holocene faulting and volcanism that include the Northwest Rift zone, the Tumalo fault, and the Rimrock fault [U.S. Army Corps of Engineers, 1983a; Nakata et al., 1992]. In the Three Sisters area, Holocene volcanic vents form a left-stepping en echelon pattern consistent with zones of right-lateral shear that cross the axis of the Cascade arc [Bacon, 1985]. The Walker Rim and Sisters-Green Ridge fault zones have been inferred to form a pull-apart basin beneath Newberry Crater [Gutmanis, 1989; Goles and Lambert, 1990] consistent with transtensional components of motion in the arc. This pattern of normal faulting interrupted by right-slip shear zones supports previous tectonic interpretations of the discontinuous and alternating grabens and half grabens in the High Cascades [e.g., Taylor, 1990; Wells, 1990; Magill et al., 1982].

Several river valleys located west of the Cascade arc are structurally controlled by northwest striking right-slip faults including faults in the Upper Willamette River and Clackamas River valleys (Figure 2) [U.S. Army Corps of Engineers, 1981a; Hammond et al., 1980; Beeson et al., 1989]. Faults along the Upper Willamette River Valley are part of the right-slip Eugene-Denio zone proposed by Lawrence [1976] and were found to offset Pleistocene gravels; although they are short and show little total displacement [U.S. Army Corps of Engineers, 1981a]. Several north- to northwest-trending zones of seismicity and crustal deformation stretch across the lower Willamette Valley and Portland Basin (Figure 2). For example, the Mount Angel zone and the Portland Hills zone are defined by earthquakes with right-slip mechanisms [e.g., Werner et al., 1992; Yelin and Patton, 1991]. Here and at other sites in the Willamette Valley, faulting and folding are recorded in Quaternary and latest Tertiary subsurface structures [e.g., Yeats, 1990a, b; Werner et al., 1992] and possibly in the late Quaternary terraces [e.g., Balster and Parsons, 1968]. Northwest-trending photo-linears and inferred young faults locate near the Gales Creek zone and along the southwestern base of Mount Hood (Figure 2). Right-slip shears of the Clackamas River fault zone deform late Quaternary lavas and project northwest from the arc towards the Portland Hills fault zone [Hammond et al., 1980; Beeson et al., 1989]. The city of Portland, Oregon, has been proposed to lie within a pull-apart basin between right-lateral strike-slip faults [Beeson et al., 1989]. Seismicity in the basin has been inferred to be associated with these faults [e.g., Yelin and Patton, 1991]. The Portland Hills-Clackamas River zone may interact with the St. Helens seismic zone, which is defined by a 100-km-long zone of earthquakes that trends north beneath the volcano and shows predominantly right-slip and normal mechanisms [Weaver et al., 1987; Ludwin et al., 1991].

Central Oregon Zone

The Central Oregon fault zone splays north from the Walker Lane, steps left (west) across the base of three northward trending range fronts and forms left-stepping grabens that project northwest into Newberry volcano (Figures 1 and 2). Overall, the zone trends about N20°W and is ~400 km in length. Our field investigations have focused on mapping and trenching the young scarps in order to obtain measurements of the displacements and ages of late Quaternary faulting at sites along the Central Oregon zone. Individual faults within the zone show mostly normal displacements; however, some faults show evidence of right-slip displacement and others left-slip displacement (Figures 4a through c). A brief description of the ages and amounts of faulting, the senses of motion, and preliminary slip rates along the zone follows.

Surprise Valley Fault. Scarps along the Surprise Valley fault stretch for 84 km and show as much as 14 m of normal separation in latest Pleistocene pluvial lake sediments [Hedel 1980, 1984] (Figure 2). The surface trace shows a slight left-stepping, en echelon pattern, which may indicate a small right-lateral component of slip. The scarp heights and estimated ages indicate that the average slip rate is ~1/2 to 1 mm yr^{-1}. Hedel [1980, 1984] maps late Pleistocene deposits on the floor of Surprise Valley that may be offset by additional right-slip faults, providing evidence for several northwest trending structures that may be young and play a role in right-lateral faulting along this zone.

Goose Lake Graben. Although scarps cannot be found along the major range-bounding faults of the Goose Lake graben (Figure 2), smaller faults on the valley floor offset Pleistocene(?) pluvial lake sediments by several meters [Pezzopane, 1993]. Faceted spurs and fault-related ridges mark the oversteepened base of the mountain front. The elevations of Plio(?)-Pleistocene lake sediments and geomorphic remnants of shorelines (1555 m, ~5100 ft) [Brown et al., 1980] are about 100 m above the estimated lowest spillover of Goose Lake (1445 m, ~4740 ft). We infer that the shoreline deposits are uplifted by repeated faulting. Trench excavations near the foot of the range reveal thick deposits of historic (more than 1 m) and Holocene(?) colluvium (more than 3 m), indicating that depositional rates may be high enough to rapidly bury or destroy young fault scarps (unpublished trench logs by authors and P. Pedone, Soil Conservation Service, Portland Oregon).

Warner Valley. Although no young scarps are recognized along the range fronts in the Warner Valley (Figure 2), tilted latest Pleistocene pluvial lake shorelines record almost 1 mm yr^{-1} of vertical deformation across the basin [Weide, 1975; Craven, 1991]. At the northern end of Warner Valley (Figure 2), aerial photos show several linear fault scarps(?) that splay across the valley floor and appear to bound some of the modern lakes and playas [Pezzopane, 1993]. Smaller scarps(?) interrupt the pluvial lake shorelines at places farther south. Faults in this valley are associated with historic seismicity; the 1968, Adel, Oregon earthquake swarm [Schaff, 1976; Couch and Lowell, 1971; Patton, 1985]. For the largest event, $m_b = 5.1$, Patton found a predominantly normal faulting mechanism with a small component of oblique slip. Assuming that slip occurred on the steeply dipping plane that strikes north, the motion was right-oblique.

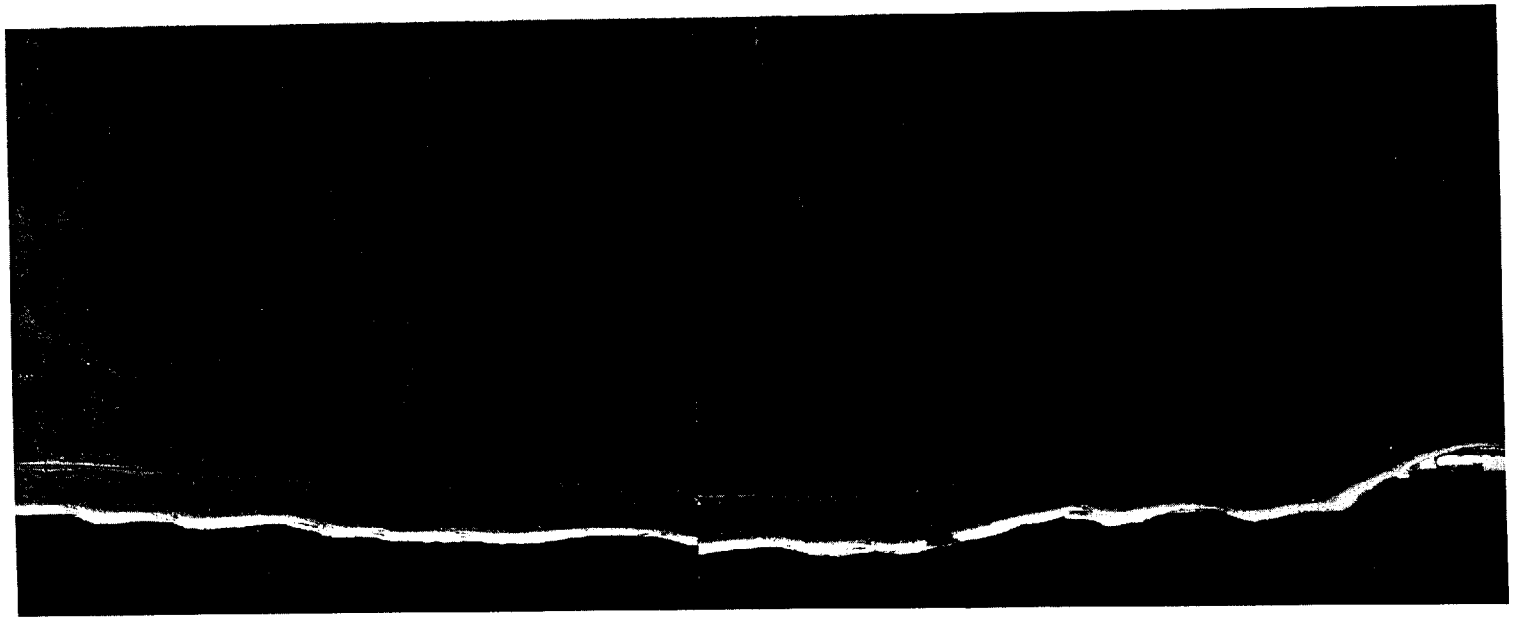

Fig. 4a. Oblique areal photograph of Holocene fault activity along the Central Oregon fault zone showing an eastward view of part of the Abert Rim fault (arrows) where it offsets young colluvium, alluvium, and latest Pleistocene pluvial lake shorelines and deposits along the western flank of Abert Rim. The free face of the young scarp appears light in color.

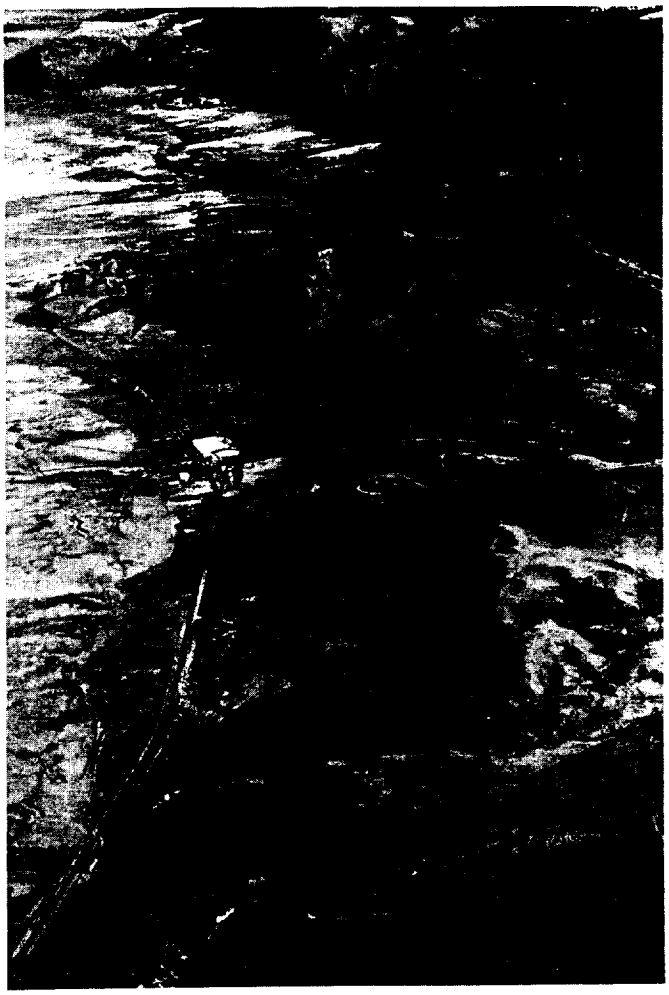

Fig. 4b. Oblique areal photograph of Holocene fault activity along the Central Oregon fault zone showing southeastward view along the left-stepping range front faults at the base of Slide Mountain (westward, off photo to right). The en echelon faulting steps left near Monument Rock (center), in places, buried by the lobe of landslide debris (left center), and continues along the base of the faceted spurs farther southeastward (arrows in distant background).

Abert Rim Fault. The Abert Rim fault exhibits almost continuous geomorphic expression for over 30 km, striking on average about N20°E and displacing late Pleistocene and Holocene lacustrine, alluvial, and colluvial deposits along the western flank of Abert Rim [Pezzopane, 1993] (Figures 2 and 4a). The surface trace is relatively segmented and zig-zags in and out of salients in the range front. The style of slip is predominantly normal; however, the surface trace takes several right steps, perhaps consistent with a small component of left-oblique motion. Scarps across debris flows that bury the lowest (~4300 ft) and presumably youngest pluvial lake shorelines average about 4 m to 5 m in height, which is representative of the scarp height along most of the zone; however, the scarp is as much as 8 m high in apparently older (late(?) Pleistocene) lacustrine and colluvial deposits [Pezzopane, 1993]. An average slip rate of 1/2 mm yr^{-1} is consistent with 8 m of separation in latest Pleistocene (~16,000 years in age) pluvial lake sediments. Preliminary analysis indicates as much as 14 m of vertical difference in the elevations of the highest, prominent wavecut shorelines along the base of Abert Rim relative to the highstand shorelines in other parts of the basin [Pezzopane and Weldon, 1990; Pezzopane, 1993], perhaps consistent with deformation rates (mostly fault slip) of 1/2 to 1 mm yr^{-1}.

Slide Mountain Fault. The Slide Mountain fault is a segment of the major range bounding fault near Winter Ridge [e.g., Russell, 1884] (Figure 2). The youngest faulting is along two segments that strike nearly E-W (Figure 4b); however, the entire zone strikes on average N60°W [Pezzopane, 1993]. A right-stepping geometry along part of the trace is consistent with a small left-lateral component of slip (Figure 4b). Scarps formed in latest Pleistocene pluvial lake deposits and younger colluvium average 6 to 7 m in height and, in places, are as much as 10 m high. Trench excavations reveal lacustrine deposits that record multiple episodes of faulting. Faulted and intensely folded lacustrine units interlayered with fault-related colluvium may indicate that repeated displacements occurred when lake levels were above the scarp, probably in Latest Pleistocene time [Pezzopane, 1993]. The scarp is buried in places by fan deposits dated at 2130 ± 90 yr B.P. (Beta-15818), providing a minimum age for the multiple-event scarp. Dividing the surface displacements (~6 to 10 m) by the

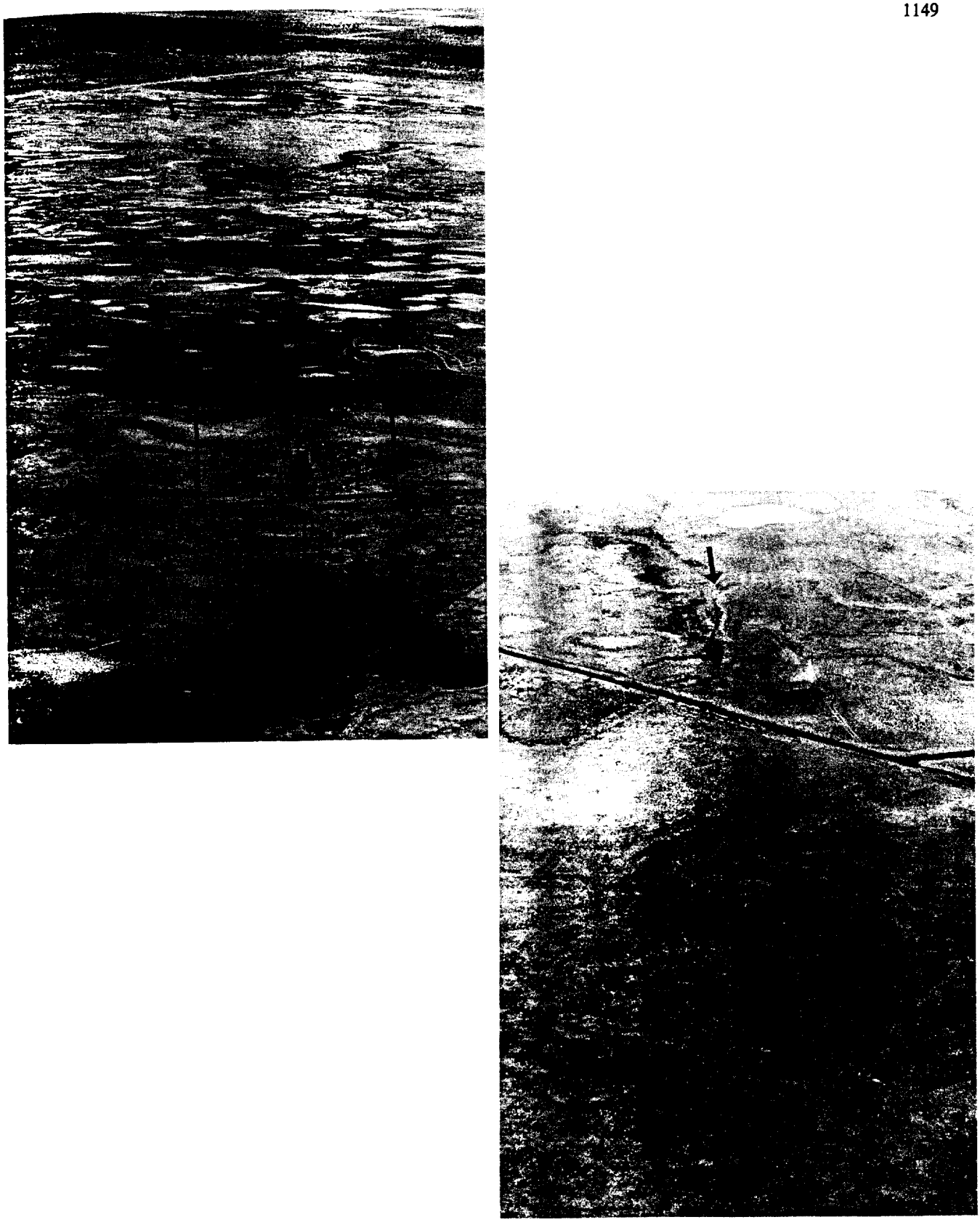

Fig. 4c. (Left) Oblique areal photograph of Holocene fault activity along the Central Oregon fault zone showing northward view of the Paulina Marsh fault (arrows along strike). (Right) Northwestward view of the southern segment (box in left photo) which shows apparent lateral separation of young stream channels.

estimated age of the displaced lacustrine sediments and colluvium (~16,000 years) results in an average slip rate between 0.4 and 0.6 mm yr^{-1}.

Ana River Fault. The Ana River fault strikes N10°W for a minimum of 3 km (Figure 2). A prominent Neopluvial shoreline [e.g., Allison, 1982] appears to have washed and buried much of the scarp. Near Slide Mountain this shoreline cuts the fan deposits dated at 2130 years old. Trenching across this fault reveals that latest Pleistocene lacustrine deposits and tephra layers are displaced ~4 m by two or more events [Pezzopane, 1993] (Figure 5a). The steep fault dip and anastomosing style of faulting seen in the trench may indicate a minor oblique component of slip. The displacement is large for such a small fault length, and we suspect this fault may connect to or be a splay of the Slide Mountain-Winter Ridge fault system. Large landslides off Winter Ridge have destroyed most of the late Pleistocene lake shorelines, along with the record of range front faulting here. However, several latest Pleistocene tephra layers in the Ana River area show evidence of young deformation [e.g., Simpson, 1990]. Ages inferred from tephra correlations and displacements measured on the surface and in trenches indicate that average fault slip rates are between 0.2 and 0.6 mm yr^{-1} for individual faults in this basin [Pezzopane, 1993].

Viewpoint – Crack-In-The-Ground Faults. The Viewpoint fault forms a 2 m scarp across all but the youngest (i.e., Neopluvial of Allison [1979, 1982]) lake shorelines (Figure 2). Trench excavations reveal several high-angle fault strands and evidence for multiple episodes of latest Pleistocene activity [Pezzopane, 1993] (Figure 5b). En echelon faulting splays left (northwest) onto the valley floor and forms small grabens that appear to control the locations of the modern playa and young volcanic centers lying to the northwest [e.g., Walker et al., 1967; Walker and MacLeod, 1991]. Crack-in-the-Ground fault, on the northern flank of the valley (Figure 2), is part of a young graben that bounds the Four Craters volcanic center [e.g., Peterson and Groh, 1964] which is mostly Holocene in age [e.g., Walker and MacLeod, 1991]. Pleistocene lava flows are vertically offset 10 m along Crack-in-the-Ground fault, and other subparallel faults in the zone each show comparable surface separation [Pezzopane, 1993]. Crack-in-the-Ground scarp is partially buried by a Holocene lava flow from Four Craters which is also offset by small fractures indicating repeated Holocene movement on the fault. Available age rela-

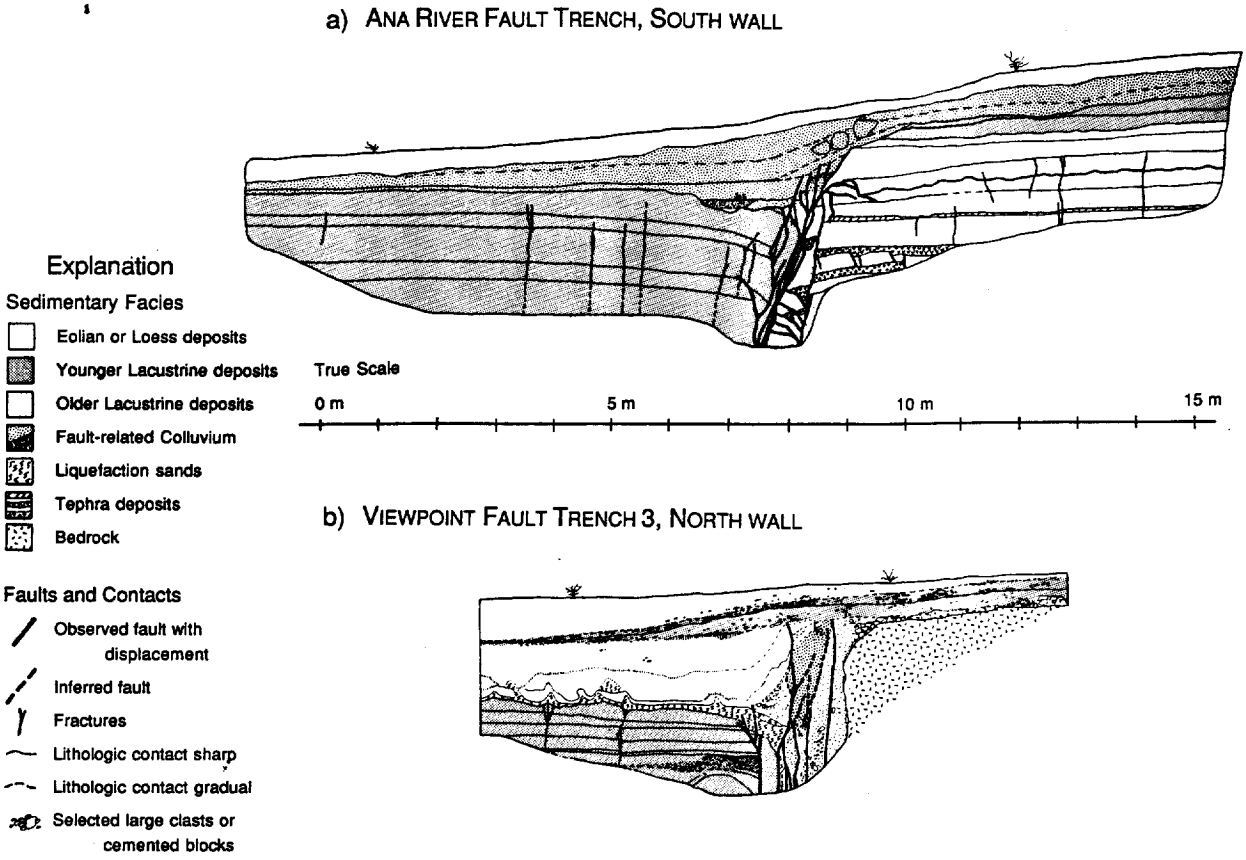

Fig. 5. Idealized logs of exposures in trench excavations across the (a) Ana River fault and (b) Viewpoint fault. At both sites, latest Pleistocene pluvial lake deposits are offset by three or more episodes of faulting which occurred along relatively steeply dipping and anastomosing zones. In each case, younger fault movements offset fault-related colluvial wedges, dikes of liquefied sands, and buried zones of intense disruption. Younger lakes, probably Neopluvial in age [e.g., Allison, 1982], occupied the basins in this region and reworked the scarps at these sites (note gentle scarp slopes), as well as others in the nearby valleys, destroying evidence for young deformation and making active faults difficult to recognize. The style of fault slip inferred from the trench excavations is normal oblique.

tions and measured displacements are consistent with slip rates ranging from 0.1 to 0.5 mm yr^{-1} across the Viewpoint and Crack-in-the-Ground fault zone.

Paulina Marsh Fault. Faults in Paulina Marsh are expressed across the valley floor for over 7 km (Figure 2 and 4c). The fault zone strikes ~N30°W, and the maximum scarp height is ~2 m [Pezzopane, 1993]. Aerial photography reveals stream channels that appear to be separated right-laterally (Figure 4c); however, to confirm this requires additional work.

Summary. The Paulina Marsh, Viewpoint, and Crack-in-the-Ground faults strike northwestward and merge into several late Pleistocene volcanic complexes south of Newberry [Walker et al., 1967; Walker and MacLeod, 1991]. Taken together, the young faulting through central Oregon forms a relatively continuous, left-stepping, en echelon zone (Figure 2). The faults splay northwestward from the Walker Lane along several major range fronts and ultimately project into the Cascade arc through active volcanic complexes including Newberry volcano. The left-stepping pattern may reflect overall right-lateral shear, which is evident where this zone ultimately merges with the Sisters zone in the Cascades (Figure 2). Major off-axis volcanoes, such as at Newberry and Mount St. Helens, appear to be located where northwest striking fault zones diverge from the axis of the Cascade arc.

Eastern Oregon Zones

The Eastern Oregon fault zones define the bases of major mountain ranges and stretch across northern Nevada into southeastern Oregon (Figures 1 and 2). The dominant zones of faulting strike north-northeast and are on trend with Holocene and historic surface ruptures of the central Nevada seismic zone [Wallace, 1984; Doser, 1988; dePolo et al., 1991]. These zones appear to be a northward continuation of activity along the central Nevada zone.

The westernmost zone consists of faults in the Smoke Creek and Black Rock deserts, Nevada, continuing into the Alvord Desert, Oregon (Figure 2). Right-oblique displacements of Pleistocene and Holocene age are distributed across faults in the Smoke Creek Desert [Bell and Slemmons, 1982b]. Normal faults offset Holocene deposits ~8 m along the Black Rock fault [Dodge and Grose, 1979]. Both graben-bounding faults in the Alvord desert show young activity [Hemphill-Haley et al., 1989; Lindberg, 1989]. Trench exposures of the Steens Fault reveal sediments younger than 2000 years that are offset ~2 m [Hemphill-Haley, 1987]. Faults along this entire zone show multiple episodes of activity and complex rupture patterns [e.g., Dodge and Grose, 1979; Hemphill-Haley et al., 1989].

The easternmost zone stretches northward along the western flank of the Santa Rosa Range, Nevada, crosses the Quinn River Valley into Oregon, and steps northeastward across the Blue Mountains into the Owyhee River area near the Idaho border [Nakata et al., 1992; Pezzopane et al., 1992] (Figure 2). Interpretation of aerial photography indicates that this zone consists of numerous en echelon scarps with differing heights and degrees of freshness. Preliminary field investigation reveals scarp heights of as much as ~6 m in Pleistocene-Holocene(?) fan alluvium, and locally, even the youngest (Late(?) Holocene) stream terraces are offset by recent faulting. Estimated scarp heights and ages of offset strata along the Smoke Creek-Black Rock-Alvord and the Santa Rosa-Quinn River-Owyhee River zones are consistent with average slip rates of 1/2 to 1 mm yr^{-1} along the zone.

It is not clear whether the Eastern Oregon zones connect to the Brothers fault zone or to a distributed zone of earthquake and fault activity that stretches northwest across western Idaho, northeastern Oregon, and southern Washington. The Brothers fault zone has been proposed to be one of four major right-slip zones which form the northwestern boundary of the Basin and Range Province in central Oregon [Lawrence, 1976]. Considerable evidence, however, indicates that the Brothers fault zone is not as active as it was in Miocene time [Priest et al.,1983; MacLeod and Sherrod, 1988]. We have found little evidence of Holocene fault activity in our preliminary investigations of the Brothers zone, whereas the zone extending across northeastern Oregon shows both Holocene fault activity and historical seismicity, as discussed below.

Olympic-Wallowa – Puget Sound Zone

Earthquakes and young faulting are distributed along a broad, northwest trending zone from southwestern Idaho, through northeastern Oregon, the Yakima fold belt, and the northern Cascades, collectively known as the Olympic-Wallowa lineament (OWL) [e.g., Raisz, 1945; Hooper and Conrey, 1989; Mann and Meyer, 1993] (Figures 1 and 2). Earthquake focal mechanisms and geologic structures along the Olympic-Wallowa zone indicate distributed right-oblique normal faulting to the south, alternating to right-lateral strike-slip and right-oblique reverse faulting farther northwest [e.g., U.S. Army Corps of Engineers, 1983b; Tolan and Riedel, 1989; Hooper and Conrey, 1989; Ludwin et al., 1991]. For example, at the southeastern end of the OWL, several northwest-striking right-slip zones alternate with normal-oblique, graben-bounding faults including the Long Valley fault system in Idaho, and the Pine Valley and Baker grabens, Oregon [e.g., Mann, 1989; Wood, 1990] (Figure 2). In places, middle to late Quaternary strata are offset as much as ~2 km [e.g., Hooper and Conrey, 1989; Mann, 1989; Mann and Meyer, 1993], and microseismicity is located along some of the currently active faults [e.g., Zollweg and Jacobson, 1986; Mann and Meyer, 1993]. Latest Pleistocene-Holocene colluvium is cut by right-oblique faults in the La Grande graben [Gehrels et al., 1980; U.S. Army Corps of Engineers, 1983b], and along the right-slip Wallula fault [Mann and Meyer, 1993]. Several northwest faults such as the Milton-Freewater and Arlington-Shuttler Butte zones [U.S. Army Corps of Engineers, 1983b] and faults in the Kittitas Valley [Waitt, 1979] displace late Quaternary strata in a right-lateral sense. Northwest toward the Cascade arc, belts of anticlines and thrust faults mark the Yakima fold belt, a region of mainly transpressive tectonics [e.g., Reidel, 1984; Tolan and Reidel, 1989; Beeson and Tolan, 1990]. Shortening occurs along thrust faults and folds such as in the Saddle Mountains area [Reidel, 1984; West and Shaffer, 1989], a seismically active region marked by mostly thrust earthquakes [e.g., Ludwin et al., 1991]. Folding and thrust faulting of Holocene deposits along the Toppenish Ridge uplift has formed scarps that indicate an average fault slip rate of ~1 mm yr^{-1} or greater [Campbell and Bentley, 1981].

Crustal earthquakes continue this zone of strike-slip and thrust faulting across the Cascade axis, for example near Mount Rainier [Crosson and Frank, 1975], into the Puget Sound region, and northward to the Canadian border [Crosson, 1972; Wilson et al., 1979; Noson et al., 1988; Ludwin et al.,

1991] (Figure 2). Folded Quaternary and Holocene strata are evidence for reverse slip along the Seattle fault in Puget Sound [Yount and Holmes, 1992], a fault which may be structurally related to uplift on the Olympic Peninsula. Offset of Holocene deposits and focal mechanisms of historic earthquakes both indicate reverse and right-slip movement on faults near the Dow and Saddle Mountains [e.g., Wilson et al., 1979]. Although few active faults have been recognized farther north on this trend, several large-magnitude crustal earthquakes near Vancouver Island yield fault-plane solutions consistent with strike-slip faulting and N-S compression [e.g., Rogers, 1979]. Many workers have recognized that the P axis orientations of mechanisms from shallow, crustal earthquakes in the Puget Sound and Vancouver Island regions are oriented generally N-S and are not parallel to the local direction of Juan de Fuca plate convergence (N65° to 70°E) [e.g., Crosson, 1972; Rogers, 1979; Spence, 1989]; however, geodetic surveys [e.g., Savage and Lisowski, 1991] on the coast of western Washington indicate the orientation of maximum compressional strain is parallel to the direction of Juan de Fuca plate convergence predicted from global models. We interpret this lack of correspondence to suggest that crustal earthquakes in the Puget Sound-Vancouver Island area are associated with northwest-trending zones of faulting that link motions in northern Oregon and western Washington with the Queen Charlotte transform system north of Vancouver Island.

CRUSTAL DEFORMATION

Contemporary strain estimates for regions in the western United States have been made from studies of seismicity, fault slip rates, tectonic models, and geodetic measurements [e.g., Minster and Jordan, 1984, 1987; Weldon and Humphreys, 1986; Eddington et al., 1987; Wells and Heller, 1988; Sauber, 1990]; however, few of these studies include data from Oregon and the vicinity. Overall, the four fault zones that cross Oregon serve to separate relatively stable lithospheric blocks to the west from the North American plate to the east (Figure 2). The largest among these is a coastal block previously referred to as the "Willamette Plate" [e.g., Magill et al., 1982; Wells and Heller, 1988; England and Wells, 1991], which encompasses most of western Oregon. We seek to infer the direction and rate of motion of this coastal block relative to "fixed" North America across the Cascades, Central, and Eastern Oregon fault zones. This is difficult because the zones are broadly distributed and consist of diverse structures. Given the orientations of the faults and the dominant style of faulting, the blocks move in a direction between west and north at an undetermined rate.

Three different methods are used in an attempt to estimate the relative velocities of blocks across the deforming zones. The orientations and styles of active faults are analyzed with the Withjack and Jamison [1986] model of oblique rifting to estimate the overall direction of motion. Moment tensor methods that utilize the orientations and displacements of Holocene faults and historic earthquakes [e.g., Kostrov, 1974; Wesnousky et al., 1982] are used to determine velocities. Traditional seismic moment tensor methods use historic seismicity data to determine the rates and directions of motion. The application of this technique is limited here, however, because the historic record is too short to span the average recurrence time of large surface-rupturing earthquakes. The moment tensor methods apply to either geologic fault displacements or earthquake moment tensor solutions [e.g., Scholz and Cowie, 1990]. Velocity estimates based on the geologic record of Holocene fault slip may be more reasonable because the record encompasses longer time intervals, yet estimates of the direction of motion are less reliable because exact slip vectors are not available or known only locally.

The mapped traces of active faults recognized along the central and eastern Oregon fault zones (Figure 6) are divided into 1-km-long segments and the average strike and displacement are recorded (Table 1). Strikes of active faults in central Oregon and northern Nevada (Figure 3f), taken as a group, span a broad range of about 100° and cluster mostly in the north and northeast directions. The dominant trends appear to match the regional late Tertiary faults with large offset (i.e., Figure 3d and 3e), whereas the northwest striking fault set, like in the Brothers zone and near Summer Lake (i.e., Figures 3a, 3b, and 3c), is not as apparent. This could be a result of sampling because normal scarps are generally easier to find. Evidence for strike-slip motion may be more difficult to recognize and preserve in the active playas here.

In the context of the Withjack and Jamison [1986] model, the active faults show a pattern that is consistent with right-lateral shear oriented 30° away from the rift trend (R), which is inferred to be oriented around N20°W (Figure 3f). Although the fault data may be incomplete, this result points to the range-bounding normal faults that strike north to northeast as the prominent players in the Holocene, which is different than the "conjugate" strike-slip style of faulting inferred from the late Tertiary fault pattern. Whereas the overall motion (N50° to 60°W) is roughly the same as that inferred from the older faults (arrows, Figures 3a through 3f), the earlier episode of faulting is characterized by only slightly smaller α values ($\alpha \leq 15°$) and rift trends (R) which are much more westward (N45° to 70°W). The Withjack and Jamison model indicates that the inferred orientations of the rift (R) and maximum horizontal extension have rotated clockwise and more northerly in the Holocene.

Withjack and Jamison [1986] model the rift (R) as a zone of weakness that underlies the crust. Perhaps this rift has a relationship to previously recognized "deep-seated fracture zones" in northwestern Nevada and southeastern Oregon [e.g., Stewart et al., 1975; Zoback and Thompson, 1978; Wallace, 1984]. Zones of feeder dikes associated with volcanism in regions of the Columbia Plateau and Basin and Range Province nearby trend on average ~N10° to 20°W [e.g., Zoback and Thompson, 1978; Hooper and Conrey, 1989]. The rift trend inferred from the pattern of active faulting (~N20°W, Figure 3f) roughly corresponds to the regional trend of the Central Oregon zone (Figure 1) and to the overall trend of the "eastern shear zone" (i.e., Figure 1, from the San Andreas system south of the Mojave Desert to the Queen Charlotte system located northwest of Vancouver Island).

The shift to a rift direction trending more northward, as seen with the Holocene fault data may correspond with studies [e.g., Zoback and Thompson, 1978; Zoback et al., 1981] which infer that Basin and Range extension has rotated as much as 45° clockwise from earlier extension directions as a result of superposition of right-lateral shear associated with development of the transform system at the Pacific-North American plate boundary [e.g., Atwater, 1970]. Alternatively, the older and more local northwest striking zones like the Brothers [e.g., Lawrence, 1976] have become less significant as greater offset develops, as younger faulting favors the northward trends of

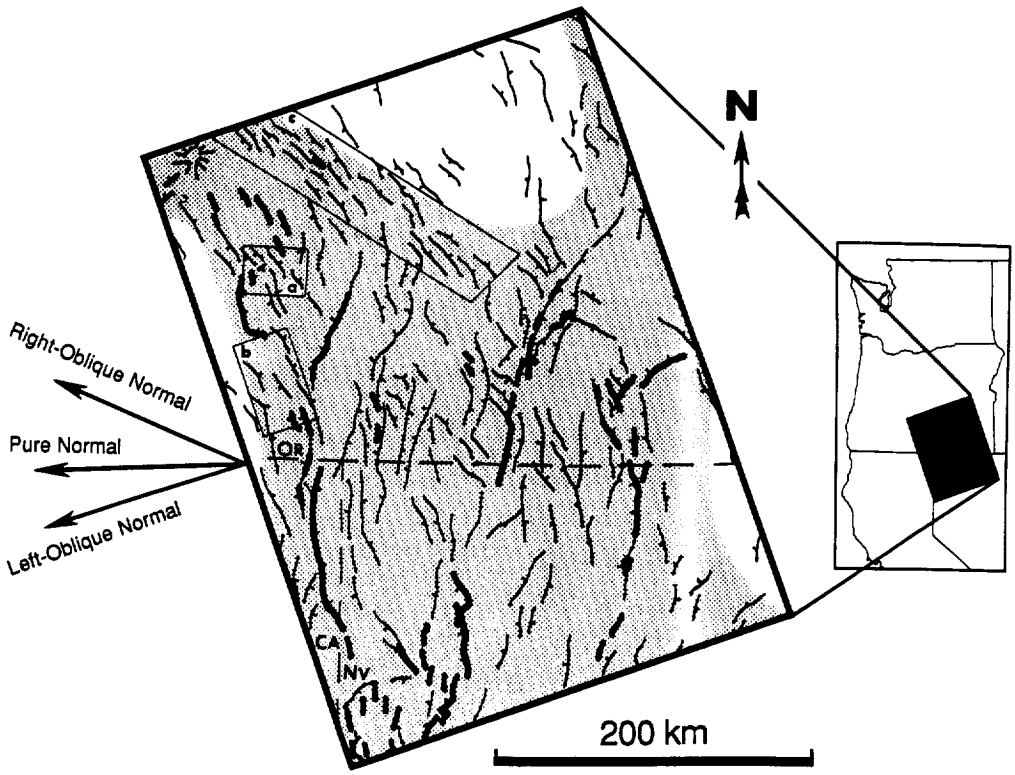

Fig. 6. Map of active faults along the central and eastern Oregon zones (bold) that are used to construct geologic moment tensors and estimate possible directions of overall crustal deformation (arrows). Late Quaternary and Holocene fault activity is from Dodge and Grose [1979], Hedel [1984], Hemphill-Haley [1987], and Pezzopane [1993]; whereas the older faults and base map are from Walker and MacLeod [1991], Jennings [1992], and Stewart and Carlson [1978]. The directions of overall crustal deformation, obtained from summing the moment tensors of active fault displacements, are shown for assumed styles of faulting, taken in a reference frame oriented parallel to the sides of the deforming volume. Seismic moment tensors are constructed from the fault strike and displacements, which are measured on the surface and in trenches (Table 1) and are assumed values of dip and rake (Table 2). Note that for pure extension to occur across the N-NW trending zone, all fault must be left-oblique. Assuming pure normal to right-oblique slip on recognized active faults in southeastern Oregon and northwestern Nevada results in overall motion oriented about N60°W ± 20°. Strikes of faults in (a) Summer Lake, (b) Summer Lake south, (c) Brothers zone, and (d), (e), and (f) the total region are summarized in Figure 3.

the Oregon fault zones (Figures 1 and 2). The Withjack and Jamison [1986] model can be used to explain the styles of faulting and directions of crustal block motions; however, the technique cannot provide information about the rate of motion across the zone or the relative contribution of faults with the most displacement. So we turn now to a seismic moment tensor approach.

Geologic Moment Tensors and Strain From Active Faulting

The scalar seismic moment M_0 quantitatively describes the size of an earthquake or shear dislocation on a fault and is directly proportional to seismic energy release and strain [e.g., Aki and Richards, 1980]. The seismic moment is defined as

$$M_0 = \mu A s, \tag{1}$$

where μ is the shear modulus, A is the area of the fault surface that slips, and s is the average amount of slip. When both the M_0 and fault slip vector are known, the moment tensor, M_{ij}^n, describes the amount and direction of slip from the nth fault or earthquake as

$$M_{ij}^n = M_0^n\left(u_i n_j + u_j n_i\right), \tag{2}$$

where u and n are unit vectors in the direction of slip and normal to the fault plane, respectively [e.g., Aki and Richards, 1980]. Assuming linear elasticity and homogeneous strain, the moment tensor can be converted to the strain tensor using Kostrov's formula. Kostrov [1974] showed that the average rate of irrotational strain ($\dot{\varepsilon}_{ij}$) in a region where earthquakes (or fault displacements) are distributed uniformly throughout a volume (V), is proportional to the sum of the moment tensors (ΣM_{ij}) of all fault displacements occurring in the volume during a time (T);

$$\dot{\varepsilon}_{ij} = \frac{1}{2\mu VT}\sum_{n=1}^{N} M_{ij}^n. \tag{3}$$

This analysis assumes that the deformation within the zone is homogeneous (no gradient of velocity parallel to strike) which neglects possible components of rotational deformation [e.g., Molnar, 1983; Jackson and McKenzie, 1988]. Paleomagnetic studies in and near Oregon show that block rotations are large-scale across regional zones and small-scale in locally complex areas, and rotation rates are greater than 1° per Ma in places [e.g., Magill et al., 1982; Wells and Heller, 1988; Stimac and Weldon, 1992]. Unfortunately, rotations are unobservable from seismic moment tensors unless the tensors are known everywhere within the deforming zone [e.g., Haines, 1982; Jackson and McKenzie, 1988]. Although we recognize rotations within the deforming zones, we do not explicitly include them in this analysis.

The approach is to construct seismic moment tensors from mapped Holocene fault ruptures (Figure 6). Field mapping, fault scarp profiling, and trench excavations [e.g., Hedel, 1984; Hemphill-Haley, 1987; Dodge and Grose, 1979; Nakata et al., 1992; Pezzopane, 1993] provide maps and information concerning the distribution, age, and amount of fault slip. This analysis does not include fault slip data from the Cascade zone, which also contributes to the rate and direction of coastal block motion. The average strike and Holocene fault displacement are described for each 1-km segment (Table 1).

TABLE 1. Displacements and Strikes for Active Faults in Central Oregon

Displacement, m	Strike, °
Surprise Valley	
2	329
2	316
2	337
2	317
1.8	355
1.8	354
1.8	32
1.8	18
1.8	335
1.8	343
5	292
5.0	288
5	309
6	353
7.0	338
2	12
2	26
1.0	4
1	4
8	302
11	351
11.0	357
11	19
11	15
10	353
10	331
10	340
9.6	354
9.6	341
9.6	9
9	329
9	4
10.6	18
10.6	20
8	17
5.0	28
2	17
2	8
2	29
14.2	354
3.7	322
4.9	338
4	291
4	334

TABLE 1. (continued)

Displacement, m	Strike, °
Surprise Valley (continued)	
3.8	351
12.5	351
0.8	16
2	326
1	12
1	23
2	354
2	333
2	331
2	348
4	36
4.9	27
4.9	9
6	22
6	5
8	352
9.7	1
1.5	28
1.5	30
2	357
2	6
2	348
2	5
2	353
2	6
2	333
2	334
2	19
2	57
2	356
2	22
2	15
2	7
2	13
2	2
2	4
2	6
2	352
2	4
2	356
2	340
2	344
1.2	5
2	349

TABLE 1. (continued)

Displacement, m	Strike, °
Surprise Valley (continued)	
2	3
2	26
2	37
2	48
2	31
8	359
8	7
16.7	6
8	15
4	25
4	309
8	344
12.4	341
8	348
6	349
6	352
6	339
6	344
0.5	298
0.5	307
0.5	324
0.5	335
6	20
6	11
6	343
6	63
7.0	11
7	19
6	3
6	6
6	24
6	348
6.0	59
6	12
6	341
6	31
9	33
12.4	32
9	19
6	333
0.5	35
0.5	37
0.5	11
0.5	337

TABLE 1. (continued)

Displacement, m	Strike, °
Surprise Valley (continued)	
0.5	21
1	44
1	50
1	52
1	48
1	59
1	63
1	78
Goose Lake	
2	4
2	314
Warner Valley	
1	355
1	350
Abert Rim	
4	209
4	209
6	195
6	200
7.8	198
6.8	163
4	212
4.8	199
4.2	168
5.8	185
5.8	161
4	228
4	214
4	172
4	212
4	226
4	201
5.0	211
5	184
5	196
5	177
5	174
Slide Mountain	
6	322
7	312
8	298
7.0	298
6.5	254
6	306
5	306
5.0	278
4	285
4	283
Ana River	
3.6	338
3.6	351
2.9	349
2.9	339
Viewpoint	
1.8	159
2.2	170

TABLE 1. (continued)

Displacement, m	Strike, °
Viewpoint (continued)	
2.2	172
2.2	166
2	168
Crack in the Ground	
7	330
8	328
10.0	318
9.0	325
8	333
8.0	350
8	323
Paulina Marsh	
1	152
1	150
1	142
1	150
1	157
1	152
1	149
1	145
Black Rock	
4	151
4	150
4	152
4	154
4	150
4	150
4	149
4	151
4	158
4	160
4	157
4	158
4	239
4	236
4	221
4	220
4	226
4	153
4	155
4	176
4	174
4	177
4	178
4	172
4	171
4	170
4	175
4	179
4	177
4	172
4	163
4	156
4	198
4	183
4	172
4	176
4	179
4	186

TABLE 1. (continued)

Displacement, m	Strike, °
Black Rock (continued)	
4	197
4	212
4	195
4	209
4	210
4	206
4	202
4	201
4	210
4	206
4	215
4	228
4	226
4	222
4	206
4	204
4	214
4	216
4	221
4	217
4	213
4	217
Steens	
2	38
2	42
2	25
2	6
1.5	10
2.5	351
1.5	344
1.7	351
1.7	25
2	358
2	8
2	0
2	336
2.2	7
2	356
2	354
2	6
2	10
2	353
2	344
2	357
2	344
2	285
2	285
2	327
2	329
2	331
2	354
2	3
2	352
2	356
2	351
2	352
2	9
2	357
2	331
2	71

TABLE 1. (continued)

Displacement, m	Strike, °
Steens (continued)	
2	68
2	55
2	63
2	51
2	53
Santa Rosa	
3	177
3	160
3	232
3	208
3	149
3	183
3	157
3	160
3	158
3	166
3	156
3	139
3	197
3	185
3	214
3	207
3	191
3	126
3	168
3	162
3	204
3	201
3	231
3	208
3	179
3	182
3	199
3	198
3	203
3	206
3	178
3	174
3	154
3	156
3	161
3	166
3	203
3	208
3	166
3	154
3	186
3	247
3	199
3	200
3	204
3	184
3	188
3	185
3	200
3	209
3	183
3	169

TABLE 1. (continued)

Displacement, m	Strike, °
Santa Rosa (continued)	
3	219
3	202
3	201
3	200
3	184
3	161
3	162
3	166
Quinn River	
3	250
3	250
3	250
3	250
3	261
3	261
3	261
3	261
3	248
3	237
3	239
3	238
3	238
3	247
3	247
3	243
3	243
3	240
3	237
3	232
3	232
3	213
3	213
3	213
3	213
3	243
3	243
3	221
3	194
3	194
3	210
3	240
3	220
3	220
3	220
3	220
3	233
3	233
3	251
3	238
3	206
3	191
3	209
3	231
3	170
3	170
3	170
3	170
3	184

TABLE 1. (continued)

Displacement, m	Strike, °
Quinn River (continued)	
3	184
3	194
3	194
3	194
3	154
3	154
3	212
3	212
3	212
3	212
3	194
3	192
3	192
3	171
3	171
3	319
3	346
3	0
3	316
3	316
3	345
3	356
3	5
3	7
3	6
3	2
3	64
3	64
3	61
3	61
3	61
3	51
3	51
3	68
3	68
3	63
3	63
3	63
3	63
3	49
3	49
3	49
3	49

Displacements (in meters, not corrected for dip) and strike azimuths (in degrees, measured clockwise from north) are listed for 1-km segments of each active fault zone (Figure 6). Maps and slip data are from Dodge and Grose [1979], Hedel [1984], Hemphill-Haley [1987], Nakata et al. [1992], Pezzopane [1993], and reconnaissance information. Sites with displacements measured from scarp profiles and trench logs are shown with decimal points. Measured displacements were extrapolated along strike to estimate slip on adjacent fault segments.

Where available, local measurements of displacement, recorded in scarp profiles or trench logs, are extrapolated along the zone and used for average slip (s). Where detailed studies have not been completed, reconnaissance information is used to estimate offset.

The moment tensors are initially constructed assuming the average fault dip is 60° and pure normal displacement (rake = –90°). The rake was varied between –60° (left-oblique) and –120° (right-oblique) in an effort to investigate the reliability and possible range of the solution (Table 2). Field evidence indicates that most of the recognized slip is normal; however, some faults show evidence for a component of right-lateral slip and others show left-lateral slip. The pattern of regional faulting favors a right-slip component, as discussed above with the Withjack and Jamison technique. The scalar moment for each Holocene rupture is calculated with equation (1), where $\mu = 3.3$ times 10^{11} dyne cm^{-2}; s is the Holocene fault displacement (corrected for fault dip); and $A = LW$, where L is the rupture length (in 1-km segments), and everywhere the same width, $W = 15$ km, which encompasses the source depths of 90% of the earthquakes in the Basin and Range Province [e.g., Doser, 1989]. These data are used with equation (2) to form geologic moment tensors for young faulting in Oregon (Figure 6 and Table 2).

Field evidence indicates that the ages of most ruptures with geomorphic expression in this region postdate the extensive latest Pleistocene pluvial lake deposits; yet, an absolute chronology based on dates from within the Oregon basins is the subject of ongoing research [e.g., Negrini and Davis, 1992; Freidel and McDowell; 1992]. However, lake level oscillations have been shown to be more or less synchronous throughout the Great Basin as evidenced by well-documented pluvial histories from diverse locations such as Lake Lahonton, Lake Bonneville, and Searles Lake, among others [e.g., Smith and Street-Perrott, 1983; Benson and Thompson, 1987]. If it can be assumed that the lacustrine deposits in Oregon are climatically equivalent to Lake Lahonton and Lake Bonneville deposits, then most of the faulting included in this analysis took place within the past 12,000 years; which is the initial value assumed for T in equation (3). In some areas, however, the faulting is late Holocene, so the time interval may be excessive. Alternatively, the penultimate lake deposits may be older, perhaps approaching ~16,000 to 20,000 years old [e.g., Negrini and Davis, 1992; Freidel and McDowell, 1992].

The deforming volume (V) has areal dimensions of 400 km by 290 km; the thickness is 15 km (Figure 6). The sides of the volume are oriented parallel to the strike of the deforming

TABLE 2. Geologic Moment Tensors of Active Faulting

			Faulting Style*								
			Right-oblique normal Rake = –120°			Pure normal Rake = –90°			Left-oblique normal Rake = –60°		
ΣM_{ij} Components†											
ΣM_{11}	ΣM_{12}	ΣM_{13}	41.1	–28.4	6.4	28.0	–16.8	3.7	7.4	–0.7	0.03
	ΣM_{22}	ΣM_{23}		31.4	3.7		55.7	6.4		65.0	7.4
		ΣM_{33}			–72.4			–83.6			–72.4
ΣM_{ij} Eigenvalues‡			λ	Trend,°	Plunge,°	λ	Trend,°	Plunge,°	λ	Trend,°	Plunge,°
Maximum			–73.1	218	85	–84.1	231	86	–72.8	269	87
Intermediate¶			65.1	320	1	63.7	115	2	65.4	91	3
Minimum			8.0	50	5	20.4	25	3	7.4	1	0
Horizontal slip azimuth§				292 (N68°W)			267 (N93°W)			251 (N109°W)	
Average of ε_{Hmax} and horizontal slip azimuth				306 ± 14 (N54°W)			281 ± 14 (N79°W)			261 ± 14 (N99°W)	

* Fault slip vectors are constructed from strikes and displacements (Table 1), assuming all faults dip 60° and rake 30° to either side of pure normal.

† Components of the geologic moment tensor summed from displacements and strikes of active faulting in central Oregon and nearby (Figure 6). Slip vectors are rotated to a reference frame with positive axes oriented: x_1 = N20°W; x_2 = N70°E; and x_3 = vertical. M_O is in units of 10^{26} dyn cm = 10^{19} Nm. The ΣM_O of 464 fault segments (Table 1) is 96.6 x 10^{26} dyn cm.

‡ Principle eigenvalues of ΣM_{ij} where λ is in units of 10^{26} dyn cm and extension is positive. Trend and plunge of the principle axes are in degrees measured positive clockwise from north and inclined from horizontal, respectively.

¶ The intermediate principle axis reflects the direction and magnitude of ε_{Hmax}, maximum horizontal extension.

§ Horizontal slip azimuth is the arctangent of the ratio of horizontal shear (M_{12}) to horizontal extension (M_{22}) and is measured in degrees clockwise from the north.

zone (oriented N20°W) inferred from the Withjack and Jamison analysis of Holocene faults (Figure 3f). This simplifies the analysis by allowing both horizontal strain components (extension and shear) to be compared with the motion (perpendicular and parallel, respectively) between the two rigid plates bounding the deforming zone [e.g., Jackson and McKenzie, 1988; Ekstrom and England, 1989].

The seismic moment tensors representing the fault data (Table 1) are summed and used with equation (3) to define the strain rate tensor (Table 2), which is diagonalized in the horizontal plane to estimate the direction and magnitude of the principal horizontal axes. Discussion focuses on the direction and rate of movement across the zone which results from slip on faults. The direction of motion between the blocks bounding the deforming zone (i.e., Western Oregon moves northwest relative to North America) is determined from the horizontal ΣM_{22} and ΣM_{12} components of the total moment tensor [e.g., Jackson and McKenzie, 1988]. In a reference frame oriented parallel to the rift direction (N20°W), positive values of ΣM_{22} indicate the western block moves in a direction S70°W relative to the eastern block. Negative values of ΣM_{12} indicate the western block moves in a direction N20°W, relative to the eastern block. Discussion focuses on the vector combination of these movements across the zone.

Most faults in the region are normal or normal-oblique with subordinate right- or left-slip components. On average, the slip vectors probably approach pure normal slip. A range of possible slip vectors is explored because exact slip vectors for all faults are not known. Placing pure normal slip (rake = −90°) on all active faults, the average motion across the zones is roughly E-W (Figure 6 and Table 2), and maximum horizontal extension is oriented N60°W. If slip is dominantly normal with a significant right-oblique component (rake = −120°), as longer-term and regional geologic evidence indicates, then motion across the fault zones is in a direction N60° to 70°W, and maximum horizontal extension is oriented N40° to 50°W. These results are compatible with those of the Withjack and Jamison analysis.

Multiplication of the horizontal strain components by the appropriate distances across the deforming zone provides an estimate of the horizontal velocities between the blocks bounding the zone [e.g., Jackson and McKenzie, 1988; Ekstrom and England, 1989]. In effect, this is similar to the Bruhn [1968] method, which averages all of the slip across a single, idealized fault in order to calculate the slip rate from the cumulative seismic moment. Placing all of the geologic moment on a fault surface that strikes N20°W and has dimensions of the N-S length of the volume (400 km) and thickness (15 km) gives an average slip rate of about 0.15 mm yr^{-1}. Relatively larger slip rates are required to make the scarps if the faults accommodate components of strike-slip motion.

We infer that this is a low minimum because we have not recognized the actual extent of faulting. For example, many young scarps are not preserved. In several places the faults splay across active playa floors, and the scarps are partially buried or destroyed by young eolian and lacustrine activity. If the characteristics of faulting follow the empirical relationships between displacement and fault length seen elsewhere [e.g., Bonilla et al., 1984], then several of the mapped fault lengths are too short, relative to the displacements recorded across the scarps. For example, trench exposures across the Slide Mountain, Ana River, and Viewpoint fault zones reveal that average displacements per event are about 2 m for each fault. These faults should have scarps, based on empirical relations, that continue for 30 to 40 km instead of 3 to 4 km. In number these are about half of the recognized faults, so we estimate that the Oregon zones probably accommodate two to five times more strain than recognized here, consistent with rates of 1/3 to 3/4 mm yr^{-1}. Additional deformation such as folding and regional warping are not included here, but also contribute to the total strain. For example, significant deformation of late Pleistocene lake shorelines is recorded in the Warner basin [e.g., Weide, 1975; Craven, 1991], which has historical seismicity [e.g., Schaff, 1976], but few recognized fault scarps.

Also, the ages and depths of faulting are likely to be less than we estimate. All of the faulting is assumed to be ~12,000 years old in our calculations; however, in places it is clear that the displacements are much younger, perhaps only 2000 years old [e.g., Hemphill-Haley, 1987; Pezzopane, 1993]. An average age of $T \approx 6000$ years or less may be more reasonable, since some scarps are older and some younger. It is difficult to estimate the depth of the deforming zone without seismicity data or other information. The common depth of nearby $M >$ 5 earthquakes in the Basin and Range is 9 km plus or minus about 3 km [Doser, 1989]. Generally, it is assumed that "large" faults break through the brittle crust [e.g., Sibson, 1982; Scholz, 1982], which, in a region with a high geotherm such as central Oregon, may be less than 10 km thick [e.g., Fournier, 1989; Vink et al., 1984]. Assuming that the depth of the deforming zone is 8 km and that most of the slip occurred in the past 6000 years, the rate increases to 1/2 mm yr^{-1} for the mapped faults alone. If as much as 2 to 5 times more strain exists, a rate of 1 to 2 mm yr^{-1} is possible. Although these results are based on information averaged over relatively long time intervals, it is useful to compare these results to those inferred from the seismic moment tensors of historic seismicity, since they are both measures of slip on faults, but sampled over very different time intervals.

Seismic Moment Tensors and Strain From Earthquakes

Focal mechanisms and seismic moments of 74 shallow crustal earthquakes located inboard of the major plate boundaries between latitudes 37°N and 51°N (Table 3) are used to calculate the moment tensors and the rates and directions of crustal strain (Figure 7, Table 4). The analysis is complete for $M \geq 5$ events that have occurred in the past 80 years, and smaller magnitude events ($M \geq 3.5$) are included where there are reliable fault-plane solutions or for regions where larger-magnitude earthquakes are lacking. Earthquakes were identified from various catalogues, notably the Preliminary Determination of Epicenters by the U.S. Geological Survey and a catalog published by the University of Washington. Earthquakes in the Basin and Range Province and Walker Lane show mostly strike-slip and normal-oblique mechanisms, such as along the central Nevada seismic zone [Doser, 1987, 1988] and northwestward into the southern Cascades [Patton, 1985; Patton and Zandt, 1991] (Figure 7). Oregon is rather quiescent seismically; however, activity increases as one passes northward into Washington. Crustal earthquakes in northern Oregon and southern Washington are commonly strike-slip and reverse, and are concentrated in the Puget Sound area, in the Cascades, and to the east. We infer that this zone of crustal transpression continues northwestward

TABLE 3. Source Parameters of Crustal Earthquakes in the Western United States

Date	Latitude, °N	Longitude, °W	M*	M_o†	Strike‡	Dip‡	Rake‡	Location	Reference§	Event
Dec. 14, 1872	48.80	121.40	7.3	(11,220)	—	—	—	North Cascades, Wash.	14	
Oct. 3, 1915	40.50	117.50	6.9	2,700	194	44	–61	Pleasant Valley, Nev.	1	p1
Feb. 3, 1916	41.00	117.80	6.5	600	194	44	–61	Pleasant Valley, Nev.	1	p2
Dec. 21, 1932	38.80	117.98	6.7	1,120	1	72	–176	Cedar Mountain, Nev.	1	c1
Dec. 21, 1932	38.68	118.21	6.6	850	347	81	–179	Cedar Mountain, Nev.	1	c2
Jan. 30, 1934	38.29	118.45	5.7	35	248	40	–91	Excelsior Mountain, Nev.	1	e1
Jan. 30, 1934	38.26	118.46	6.1	140	248	40	–91	Excelsior Mountain, Nev.	1	e2
June 15, 1936	46.00	118.30	6.4	(501)	—	—	—	Milton-Freewater, Ore.	14	
June 23, 1946	49.80	125.30	7.3	(11,220)	228	85	–12	Vancouver Island	13	
July 6, 1954	39.29	118.36	6.2	260	360	60	–115	Rainbow Mountain, Nev.	2, 3	a
July 6, 1954	39.20	118.40	6.1	170	345	70	–157	Rainbow Mountain, Nev.	2, 3	b
Aug. 24, 1954	39.35	118.34	6.6	830	355	50	–145	Rainbow Mountain, Nev.	2, 3	c
Aug. 31, 1954	39.72	118.47	5.8	54	22	55	–160	Rainbow Mountain, Nev.	2, 3	d
Sept. 1, 1954	39.36	118.40	5.5	(22)	20	70	–42	Rainbow Mountain, Nev.	3	e
Dec. 16, 1954	39.20	118.00	7.1	5,000	350	60	–150	Fairview Peak, Nevada	2, 3	f
Dec. 16, 1954	39.67	117.87	6.7	980	350	50	–90	Dixie Valley, Nevada	3	g
Dec. 16, 1957	49.80	126.50	6.0	(125)	248	78	17	Vancouver Island	13	
March 23, 1959	39.43	117.99	5.7	460	2	45	178	Dixie Valley, Nevada	2, 3	h
June 23, 1959	38.92	118.89	5.6	260	310	68	–138	Schurz, Nevada	2, 3	i
Sept. 17, 1961	46.02	122.12	5.1	(6)	155	68	–172	southern Washington	11	2
Nov. 6, 1962	45.64	122.59	5.2	6.8	4	69	–105	Portland, Oregon	10	20
Sept. 12, 1966	39.43	120.17	5.8	87	43	76	–11	Truckee, California	4	
April 29, 1968	39.50	122.10	4.4	2.1	129	85	–130	northern California	10	85
May 30, 1968	42.30	119.80	5.1	1.4	1	70	–109	Adel, Oregon	10	6
June 3, 1968	42.20	119.80	4.9	1.2	176	62	–84	Adel, Oregon	10	95
July 6, 1968	41.00	117.40	5.7	1.7	341	59	–132	Battle Mountain, Nev.	10	99
Nov. 1, 1968	51.00	124.10	4.5	(0.7)	65	30	72	Vancouver Island	13	
April 27, 1971	39.40	120.20	4.4	0.19	151	78	170	northern California	10	89
July 5, 1972	49.45	127.18	6.0	(125)	154	89	163	Vancouver Island	13	
March 3, 1973	41.80	118.50	4.6	0.8	344	52	–96	northwestern Nevada	10	96
July 18, 1973	46.83	121.81	4.0	(0.1)	318	83	142	southern Washington	11	7
Jan. 6, 1974	41.12	121.49	4.1	0.4	333	82	–110	California Cascades	10	86
April 20, 1974	46.77	121.57	4.9	(3)	27	87	18	southern Washington	11	9
March 31, 1975	49.30	126.00	5.4	(16)	161	83	137	Vancouver Island	13	
Aug. 1, 1975	39.50	121.50	5.7	57	180	65	–70	Oroville, California	9	
Aug. 6, 1975	39.48	121.52	4.7	2.2	0	38	–85	Oroville, California	10	10
Nov. 30, 1975	49.20	123.60	4.9	(3)	87	41	99	Vancouver Island	13	
April 13, 1976	45.22	120.77	4.8	0.78	130	70	130	Deschutes Valley, Ore.	10	11
June 24, 1976	40.42	120.58	4.2	0.44	131	70	148	northern California	10	93
July 6, 1976	39.40	121.60	4.1	0.014	337	84	–159	Oroville, California	10	91
May 23, 1978	40.87	117.26	4.6	0.8	49	70	–60	Battle Mountain, Nev.	10	14
Aug. 1, 1978	41.45	121.88	4.6	2	25	79	–38	California Cascades	10	17
Sept. 6, 1978	45.37	121.71	3.4	(0.02)	350	90	180	northern Oregon	11	13
Oct. 4, 1978	37.39	119.49	5.8	17.8	343	45	–90	Wheeler Crest, Calif.	6	4
April 1, 1980	46.21	122.19	4.9	(3)	35	55	–80	southern Washington	12	
April 1, 1980	46.21	122.19	4.9	(3)	232	83	45	southern Washington	12	
April 8, 1980	39.50	119.18	4.7	1.1	8	52	–104	west central Nevada	10	53
April 28, 1980	41.86	118.91	4.1	0.3	14	56	–102	northwestern Nevada	10	54
April, 30, 1980	46.21	122.17	4.9	(3)	270	50	–90	southern Washington	12	
May 2, 1980	46.22	122.19	4.8	(2)	285	84	83	southern Washington	12	
May 4, 1980	46.22	122.19	4.9	(3)	254	76	85	southern Washington	12	
May 25, 1980	37.51	119.40	6.1	187	18	61	–15	Mammoth Lakes, Calif.	5	
May 25, 1980	37.17	119.35	6.1	83	283	90	180	Mammoth Lakes, Calif.	6	16
May 27, 1980	37.38	119.82	6.2	103	25	65	–6	Mammoth Lakes Calif.	5	
Nov. 28, 1980	39.31	120.43	5.2	1.3	346	64	–94	northern California	10	72
Feb. 14, 1981	46.35	122.24	5.5	(22)	355	84	–173	southern Washington	11	14
April 29, 1981	39.27	119.77	4.2	0.045	144	89	–150	west central Nevada	10	55
May 28, 1981	46.53	121.39	5.0	(4)	325	85	170	southern Washington	11	15
Sept. 30, 1981	37.01	119.02	5.8	34.1	291	90	180	Mammoth Lakes, Calif.	6	23

TABLE 3. (continued)

Date	Latitude, °N	Longitude, °W	M^*	M_0†	Strike‡	Dip‡	Rake‡	Location	Reference§	Event
Dec. 1, 1981	38.62	118.19	4.5	0.25	226	58	−62	west central Nevada	10	65
Dec. 19, 1981	38.63	118.21	4.4	0.11	62	56	−55	west central Nevada	10	66
Jan. 24, 1982	37.45	117.82	4.3	0.12	322	74	134	southwestern Nevada	10	67
June 21, 1982	41.16	121.94	4.2	0.25	173	58	−54	California Cascades	10	74
Sept. 3, 1982	39.56	122.56	4.0	0.032	0	51	−86	northern California	10	75
Sept. 24, 1982	37.85	118.12	5.4	3.6	341	78	−167	southwestern Nevada	10	68
April 11, 1984	47.53	120.18	4.3	(0.4)	116	45	150	central Washington	11	17
Nov. 23, 1984	37.48	118.65	5.9	47.7	208	87	10	Round Valley, Calif.	7	
Jan. 24, 1985	38.14	118.84	5.3	0.48	5	78	−174	east central California	10	71
Feb. 10, 1985	45.70	119.63	3.9	(0.09)	128	80	−160	northern Oregon	11	19
July 20, 1986	37.56	118.44	5.9	(89)	300	71	−164	Chalfant Valley, Calif.	8	f
July 21, 1986	37.54	118.44	6.3	(355)	155	60	−180	Chalfant Valley, Calif.	8	m
July 31, 1986	37.59	118.47	5.7	(45)	345	90	160	Chalfant Valley, Calif.	8	a
Dec. 2, 1987	46.68	120.67	4.3	(0.4)	112	51	112	southern Washington	11	21
Dec. 24, 1989	46.65	122.12	4.9	(3)	267	66	140	southern Washington	12	
April 14, 1990	48.84	122.16	5.0	(4)	5	50	41	northern Washington	12	
Feb. 23, 1991	49.45	126.95	4.9	(3)	20	75	−110	Vancouver Island	12	

* Refer to reference for magnitude scale used.

† M_0 is in units of 10^{23} dyn cm = 10^{16} Nm. Parentheses indicate M_0 is calculated from M with equation (4).

‡ Strike, dip, and rake are in degrees measured positive clockwise from north and right-handed.

§ Source parameters are taken from published studies keyed by number. 1 is Doser [1988]; 2 is Doser [1987]; 3 is Doser [1986]; 4 is Wallace et al. [1981]; 5 is Barker and Langston [1983]; 6 is Ekstrom and Dziewonski [1985]; 7 is Barker and Wallace [1986]; 8 is Cockerham and Corbett [1987]; 9 is Langston and Butler [1976]; 10 is Patton and Zandt [1991]; 11 is Ludwin et al. [1991]; 12 is R. Ludwin, written communication; 13 is Rogers [1979]; 14 is Noson et al. [1988].

across Puget Sound and Vancouver Island. All crustal earthquakes used in this analysis fall within the broad and distributed zone of mapped active faults (stipple, Figure 7) and lie away from plate boundaries and above the subducting slab. Crustal earthquakes along this eastern shear zone, together with mapped active faults, provide evidence for a broad, distributed zone of active faulting about 1400 km in length.

The seismic moment tensors are from focal mechanisms and seismic moments determined from mostly waveform modeling and moment tensor inversions (sources listed in Table 3). For some events, the focal mechanisms are from first-motion studies, and, the magnitudes (M) are converted to seismic moment (M_0) (parentheses, Table 3) using the relation

$$\log M_0 = 1.5M + 16.1 \quad (4)$$

[Hanks and Kanamori,1979; Kanamori,1983]. No attempt was made to distinguish between various magnitude scales listed by the references. Equation (4) is valid for earthquakes that encompass a wide range of magnitudes (mainly $M > 5$). This relation probably overestimates M_0 for events with $M < 5$, however; the smaller events contribute little to the moment tensor sums, relative to the larger magnitude events. As a result, errors in M_0 values are estimated to be a factor of 3 for events where M_0 was calculated from M. In most cases, strikes, dips, and rakes are taken directly from lists of fault-plane solutions; however, some rakes had to be determined from the mechanisms.

Earthquakes along the zone are divided initially into four volumes; each 15 km thick, with areal dimensions 350 km by 450 km (Figure 7). These are chosen to separate the Vancouver Island events (Figure 7a) from the central Washington events (7b), and the Basin-and-Range-type normal events in northern Nevada and southern Oregon (7c) from a mixture of strike-slip and normal events in central Nevada and the Walker Lane (7d). A reference frame oriented parallel to the rift direction (R = N20°W inferred from the Withjack and Jamison analysis of Holocene faults, Figure 3f, and the trend of the eastern shear zone, Figure 1) is used to simplify the analysis. Summing the seismic moments from historical earthquakes in each volume, the M_{22} and M_{12} components indicate that combined extension and shear, respectively, contributes to the overall direction of motion which ranges from E-W to about N20°W (Figure 7a through 7d).

Summing the tensor components, but weighting each mechanism equally (i.e., average of slip vectors) rather than by M_0, changes the estimated displacement direction as much as 30° in some cases (dashed vectors, Figure 7). Though the record may be incomplete and the results are somewhat biased toward the few large-magnitude events, the overall motion across the zone is consistently northwestward.

The summed seismic moment tensors of earthquakes that occurred in the past 80 years (Table 4) are diagonalized and used with equation (3) to estimate the rates of horizontal extension and shear (Table 5) by multiplying the horizontal strain components by the distances across the deforming volumes [e.g., Wesnousky et al., 1984; Jackson and McKenzie, 1988]. The rates range from 1 to 4 mm yr^{-1}, except for the central Washington region which is 0.01 mm yr^{-1} (Figure 7 and Table 5). Adding the seismic moments of two, pre-network events in central Washington: the $M = 7.3$, North Cascades, Washington earthquake of 1872 (assuming it was a shallow, crustal event) and the $M = 6.4$, Milton-

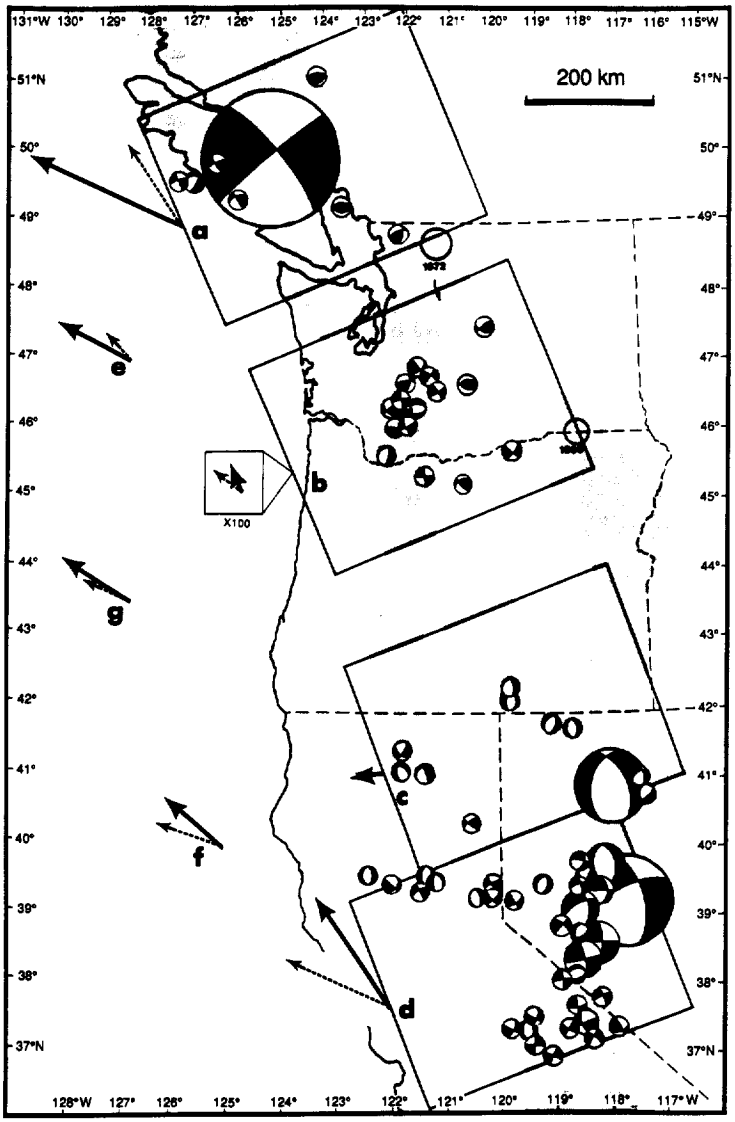

Fig. 7. Map of lower hemisphere focal mechanisms of crustal earthquakes (positioned above their epicenters) that occurred in the western Basin and Range Province and the Pacific Northwest between 1872 and 1991 (Table 3). Aerial dimensions of seismogenic volumes equal in size (350 km by 450 km by 15 km thick) are positioned to enclose the events used to calculate crustal strain across the intraarc and backarc fault zones (stipple). Velocities across the deforming zones (solid vectors, see V_{15} in Table 5) are shown for earthquakes in (a) Vancouver Island; (b) Central Washington; (c), Southern Oregon and Northern Nevada; (d) Central Nevada and Walker Lane; (e) the sum of the two northernmost volumes; (f) the sum of the two southernmost volumes; and (g) the combination of all earthquakes along the entire zone. The average slip vectors (dashed vectors) are not weighted by the seismic moments. Focal mechanisms are plotted with their area proportional to their seismic moment. An event with moment equal to 10^{20} Nm would be represented by a symbol of radius 100 km. Earthquakes with scalar moments smaller than 3×10^{18} dyn cm are plotted as symbols of constant size. The seismic moment tensors from historical earthquakes in each volume are rotated to a reference frame with axes parallel to the edges of the volume (x_1 = N20°W, x_2 = N70°E, x_3 = vertical) and summed (Table 4). The M_{22} and M_{12} components indicate that combined horizontal extension (M_{22} is positive) and dextral shear (M_{12} is negative), respectively, contribute to the overall directions of motions across the zones (vectors), which range from E-W to about N20°W. Rates of motion across the zone range from less than 1 mm yr^{-1} to as much as 7 mm yr^{-1}, although a reasonable average is ~3 ± 1 mm yr^{-1} (see Table 5).

TABLE 4. Seismic Moment Tensors of Historic Seismicity

Regions in Figure 7	n*	ΣM_{tot}†	Components of ΣM_{ij} †			Eigenvalues of ΣM_{ij} ‡		
			ΣM_{11}	ΣM_{12} ΣM_{22}	ΣM_{13} ΣM_{23} ΣM_{33}	Maximum – –	Intermediate Trend,° Plunge,°	Minimum – –
a: Vancouver Island	7	11.5	–7.3	–8.3	2.5	11.4	–11.4	0.02
				7.7	0.1	294	203	45
					–0.4	4	12	77
b: Central Washington	18	0.06	0.003	–0.03	–0.01	0.04	–0.03	0.01
	20	11.8**		0.001	0.004	137	44	281
					–0.004	15	10	71
c: Southern Oregon	12	3.3	–0.1	–0.9	0.9	3.3	–3.3	0.0
				3.0	0.7	104	206	12
					–2.9	5	70	20
d: Northern Nevada	37	11.1	2.6	–7.1	2.8	9.3	–8.4	–0.9
				1.7	2.4	317	226	49
					–4.2	2	42	48
e: Regions a and b	25	11.6	–7.3	–8.3	2.4	11.4	–11.4	0.02
	27	23.4**		7.7	0.1	294	203	45
					–0.4	4	12	77
f: Regions c and d	49	14.4	2.4	–8.1	3.7	11.7	–10.9	–0.8
				4.7	3.2	311	221	41
					–7.1	0	52	38
g: Regions e and f	74	25.9	–4.8	–16.4	6.1	22.2	–18.9	–3.3
	76	37.8**		12.4	3.3	301	211	31
					–7.5	1	31	59

† Components of the seismic moment tensor summed from the focal mechanisms and seismic moments from n earthquakes in each volume (Figure 7), rotated to a reference frame with axes oriented: x_1 = N20°W; x_2 = N70°E; and x_3 = vertical. Positive values are elongation. M_0 is in units of 10^{26} dyn cm = 10^{19} Nm.

‡ Principle eigenvalues of ΣM_{ij} where λ is in units of 10^{26} dyn cm and extension is positive. Trends and plunges of the principle strain axes are in degrees measured positive clockwise from north and inclined from horizontal, respectively.

* The value n is the total number of earthquakes used in the seismic moment tensor sum.

** Total seismic moment including the 1872, North Cascades and the 1936, Milton-Freewater earthquakes (not included in the component sums or eigenvalues).

Freewater event of 1936 (both summarized by Noson et al. [1988] and Ludwin et al. [1991]); increases the historic rate here to ~4 mm yr^{-1}, if they have the same style as the more recent seismicity.

Combining earthquakes in the two northernmost boxes into one volume (Figure 7e) and those in the two southernmost boxes into another volume (Figure 7f), each equal in size (700 km by 450 km), the directions of relative motion across the zone are between N45° to 70°W, and the rates are about 2 mm yr^{-1} (Table 5). Placing the seismic moment summed from all 76 earthquakes (Table 4) onto one fault surface (e.g., methods of Bruhn [1982]), which strikes N20°W and has dimensions 1400 km in length by 15 km in width, reveals that overall crustal motion is in a direction N60° to 65°W at an average rate of 2 mm yr^{-1} (Figure 7g).

Many authors have estimated an uncertainty of a factor of 2 to 3 in their cumulative moment tensors [e.g., Wesnousky et al., 1984; Molnar and Deng, 1984; Jackson and McKenzie, 1988; Ekstrom and England, 1989]. Our results for individual zones vary by a factor of three (Table 5). So we estimate that uncertainties in the moment release rates determined in this study are similar. Plate motion directions determined from the strain tensors probably vary by as much as plus or minus 30°, judging from uncertainties in the focal mechanisms and from being heavily weighted toward only a few large-magnitude events.

The historic record of seismic moment release records an average of ~2 mm yr^{-1} of slip along the entire eastern zone, which is a result of earthquakes in zones mainly to the north and to the south of Oregon. The seismic moment sum of all

TABLE 5. Directions and Rates of Crustal Deformation Estimated From Faulting and Earthquakes

	Slip Azimuth†		Strain Rates‡		
	Direction	Range	V_{15}	V_{10}	Eig_{10}
*From Withjack and Jamison Model**					
Late Tertiary Faults, Summer Lake	300°(N60°W)	± 30°			
Late Tertiary Faults, Brothers zone	295°(N65°W)	± 30°			
Late Tertiary Faults, Offset > 300 m	295°(N65°W)	± 30°			
Active Faults, Central Oregon	310°(N50°W)	± 30°			
From Moment Tensors and Strain‡					
Active Faults, Central Oregon	271°(N89°W)	± 20°	0.1	0.4	1.5
Historic Earthquakes, Vancouver Is	297°(N63°W)	± 30°	4.4	6.6	4.1
Central Washington	338°(N22°W)	± 30°	0.01	4.3	3.5
Southern Oregon	267°(N93°W)	± 30°	0.8	1.3	1.2
Northern Nevada	327°(N33°W)	± 30°	3.5	5.2	3.3
Regions a+b	297°(N63°W)	± 20°	2.2	6.6	6.2
Regions c+d	310°(N50°W)	± 20°	2.0	3.0	2.1
Regions e+f	303°(N57°W)	± 10°	2.1	4.6	4.0

† Horizontal slip azimuth is the overall direction of motion accommodated by the deforming zone listed as both azimuth (measured in degrees clockwise from north) and direction (in parentheses). Ranges of slip azimuths are estimated from the differences between the average slip vectors (not weighted by moment) and slip azimuths from the moment tensor sums (dashed and solid slip vectors in Figure 7). If the average slip vector and the vector weighted by moment are similar, we infer less uncertainty.

‡ Horizontal crustal strain rates (in mm yr^{-1}) across the eastern shear zone estimated from moment tensors of active faulting and historic earthquakes (Tables 2 and 4). The values V_{15} and V_{10} are the vector combination of the horizontal velocities calculated from the horizontal components of the moment tensor sums, assuming that the depth of the seismogenic volume is $W = 15$ km and $W = 10$ km, respectively. Eig_{10} is the horizontal velocity calculated from the principle horizontal eigenvalue of the moment tensor sum, assuming that $W = 10$ km. For active faults, the value V_{15} assumes that $T = 12{,}000$ years; V_{10} assumes that $T = 6{,}000$ years; and Eig_{10} assumes that $T = 6{,}000$ years and the geologic moments are a factor of 3 larger than observed. For historic earthquakes, $T = 120$ years and seismic moments from the 1872 and 1936 events are included in both V_{10} and Eig_{10}, but not V_{15}.

* The Withjack and Jamison [1986] model uses fault orientations (Figures 3 and 6) to determine styles of faulting and directions of motions accommodated by the zones. Uncertainties in the directions are estimated from the analyses and assumptions mentioned in text.

historic earthquakes in and near Oregon (converting M to M_0 using equation (4) for ~5000 events with M between 3.8 and 6.1) amounts to the strain released in a single $M_W = 7$ earthquake. Given that the earthquake record spans only 120 years and there are no surface rupturing events, this data set probably underestimates the rates of motion across the zone. Several workers have inferred long-term deformation rates from estimates of late Teriary and younger extension. For example, values of 15% to 17% extension have been proposed for this region [e.g., Wells and Heller, 1988], which averaged over the past 10 Ma across a zone 300 km wide, is consistent with an overall extension rate of about 5 mm yr^{-1}. This result is more compatible with the recognized activity of Quaternary faults, wherein the maximum scarp heights (~10 m) measured in latest Pleistocene and Holocene deposits (~10,000 years old) along several of the Oregon fault zones is consistent with ~1 mm yr^{-1} of slip across each zone, adding to ~4 mm yr^{-1} across the entire zone. These rates are similar to those calculated for active seismic zones in the Basin and Range Province nearby [e.g., Eddington et al., 1987; Minster and Jordan,

1984]. The historic seismicity record provides adequate data to estimate the direction of motion, which agrees well with the orientation inferred from the longer-term fault data.

DISCUSSION

It is reasonable to suspect that not all of the late Quaternary fault activity has been recognized. The dense vegetation and fast erosion rates in western Oregon and Washington make it difficult to find evidence of young faulting. Likewise, along the Brothers zone, for example, young faulting may be distributed across the numerous structures along the zone, and the small and diffuse scarps may not be preserved. Although we may have missed some smaller faults, the major throughgoing zones east of the Cascade volcanic arc are recognized. The evidence presented above is consistent with northwestward motion of western Oregon and vicinity with respect to North America across a distributed zone of extension and dextral shear associated with active faulting and crustal earthquakes inboard of the plate boundaries. Right-lateral shear across faults east of the Sierra Nevada reduces the amount of shear that is required to account for the total Pacific-North American plate motion along the transform boundary in coastal California [e.g., DeMets et al., 1987]. In a similar way, the orientation and amount of right-lateral shear and extension that crosses the northwestern Basin and Range carries a significant impact for the direction and magnitude of convergence between the Juan de Fuca and North American plates.

Assuming rigid plates, the Oregon zones are idealized into faults that separate relatively "stable" blocks (Figure 8). Motions across the individual fault zones are assembled from the faulting and seismicity analyses presented above. Overall, the throughgoing zone strikes roughly parallel with the plate boundaries to the west at ~N10° to 20°W and accommodates mostly oblique motions. Fault slip in central Nevada, however, produces motions roughly parallel to the San Andreas system, whereas, motions in Oregon are relatively more westward. This is illustrated best by earthquakes in Nevada and southern Oregon (Figures 7c versus 7d), which are located where the pattern of faulting becomes more distributed and fan-shaped. This large variation in slip direction occurs near the same latitude but in the region just inboard of the Mendocino Triple Junction, and perhaps in response to plate boundary related tectonics.

In an attempt to integrate the results of this study with the plate boundary tectonics, the kinematics of faulting are shown in a velocity diagram (Figure 9). If the intraarc and backarc fault zones accommodate ~4 mm yr^{-1} of motion in a direction N35° to 70°W, then western Oregon and the northern Sierra Nevada move northwest relative to North America across the eastern shear zone. The northwestward motion of western Oregon serves to rotate the orientation of Juan de Fuca plate convergence 10° to 20° clockwise, in direction almost normal to the axis of trench, while increasing the rate of convergence by ~3 mm yr^{-1} (Figure 9). Faulting along the eastern shear zone may account for nearly all of the oblique component of Juan de Fuca plate convergence, yet from available evidence it seems that relatively more motion (~1 cm yr^{-1}) is documented on faults south of Oregon. The relatively larger rate of northwestward motion in northern California (shown with VLBI vectors, Figure 9) may serve to rotate western Oregon westward as indicated by paleomagnetic measurements [e.g., Wells and Heller, 1988].

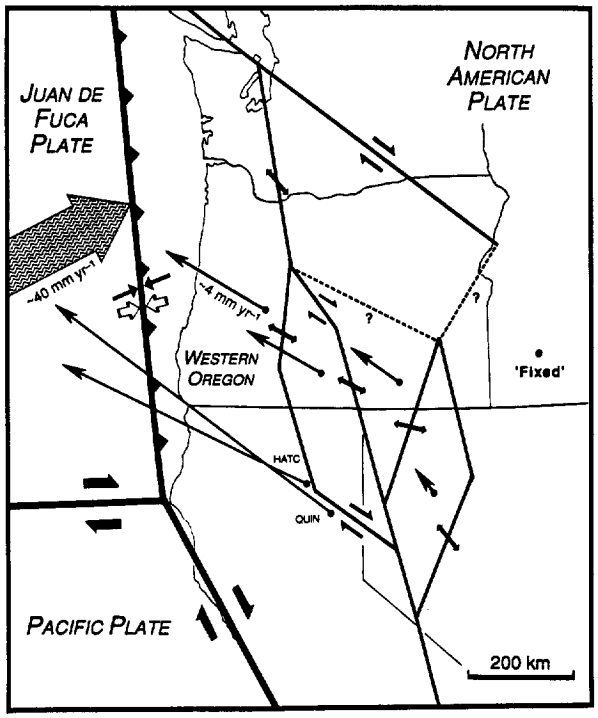

Fig. 8. Simplified tectonic map of active fault zones in Oregon and nearby regions. Idealized fault zones (lines) and directions of motion across the individual zones (small arrows) illustrate the tectonic relationships and kinematics of crustal deformation. The directions and magnitudes of the integrated motion (arrows with base points) of faults east of the plate boundaries assume North America is held fixed. The VLBI stations HATC and QUIN record ~10 mm yr^{-1} of motion and are shown in their approximate position with 95% confidence error ellipses [from Sauber, 1990]. On the basis of historic earthquake moment tensors and the styles and maximum slip rates of faults in Oregon, the overall zone accommodates motion in a direction N60°W ± 25° at rates of ~ 4 mm yr^{-1}. Dextral shear and extension across this "eastern shear zone" can account for a significant portion of the lateral component of the Juan de Fuca plate motion relative to the North American plate. If the Oregon zones accommodate ~10 mm yr^{-1}, as the VLBI measurements indicate, directions of convergence at the subduction zone become nearly normal to the trench (open arrow).

Paleomagnetic measurements record clockwise rotations of the continental margins of western Oregon and Washington, which are consistent with components of dextral shear that appear to increase as one moves westward from the Cascade arc to the coast [e.g., Magill et al., 1982; Wells, 1990]. Some models of this distributed deformation imply that a large component of shear is accommodated by quasi-continuous deformation and northward translation of the coast at rates of ~15 mm yr^{-1} [e.g., England and Wells, 1991]. Hence, much of the strain that passes inboard and north of the triple junction may not be accommodated by rigid block motions, but rather, by structures near the convergent boundary, which are widely distributed and difficult to detect. Alternatively, the clockwise

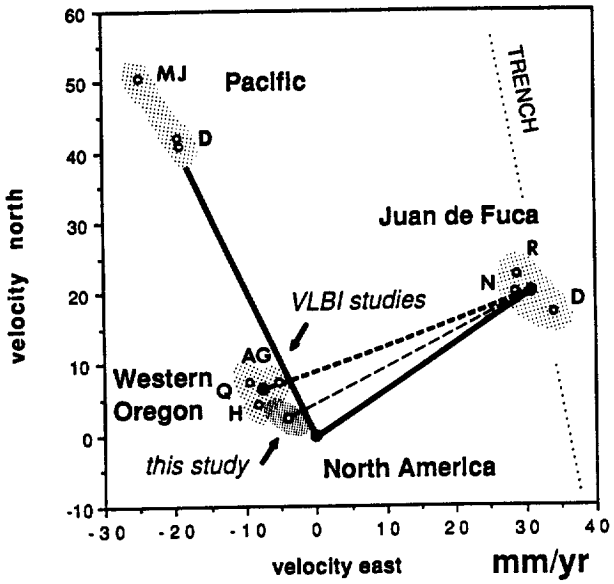

Fig. 9. Velocity vector diagram for Western Oregon relative to the North American and Juan de Fuca plate motion. This assumes that Western Oregon behaves as a relatively rigid block that is separated from the North American plate along the intraarc and backarc shear zones and from the Juan de Fuca plate along the subduction interface. Velocity components are calculated for a position at 44°N - 124°W, assuming the North American plate is held fixed. Linear velocity vectors for the various plates are calculated from the best fit Euler poles as follows. Pacific plate: DeMets et al. [1990] (D) and Minster and Jordan [1978] (MJ); Juan de Fuca plate: DeMets et al. [1990] (D), Riddihough [1984] (R), and Nishimura et al. [1984] (N); Western Oregon: Sauber [1990] (H and Q) and Argus and Gordon [1991] (AG). If faults inboard of the plate boundaries along the eastern shear zone accommodate ~1 cm yr^{-1} in a direction N60°W ± 10°, as VLBI measurements at HATC and QUIN (H and Q, respectively) indicate, then relative convergence between western Oregon and the Juan de Fuca plate (~N70°E, 42 mm yr^{-1}, thick dashes) is nearly normal to the axis of trench (~N7°W, dotted). The direction of convergence is slightly more oblique if Oregon faults accommodate only 5 mm yr^{-1} in the same direction (~N65°E, 40 mm yr^{-1}, thin dashes).

rotations may arise from a "barn door" style of rotation consistent with a pivot point west of the northern Cascades, perhaps near Puget Sound.

On a regional scale, the connection between the tectonic elements may not be as simple as portrayed. For example, dextral shear that enters the Oregon Cascades may leak motion westward to the convergent margin. The two most likely areas where this could happen are through the southern Cascades, just north of the Mendocino Triple Junction, or through the central Cascades to link with zones of dextral shear offshore western Oregon or northward in Puget Sound (Figures 1 and 2). For example, dextral shear across the Walker Lane system may pass through the Lassen region (west-trending zone of earthquakes in Figure 7d) [e.g., Klein, 1979] and connect, or step over, across northern California to the San Andreas system near the Mendocino Triple Junction. Faults near, but east of, the Mendocino Triple Junction [e.g., Herd, 1978; Kelsey and Carver, 1988] are inferred to continue dextral shear from the San Andreas system northward, perhaps to merge into the Cascadia plate boundary system or with transform structures farther offshore. Likewise, regional dextral shear in the northwestern Basin and Range Province east of the Oregon Cascades may cross the volcanic arc and western Oregon to link with active dextral shear zones offshore Oregon [Appelgate et al., 1992; Goldfinger et al., 1992a, 92b]. Few young faults have been found along either of these paths. In Washington, however, right-slip zones such as Mount St. Helens, and in particular the Olympic-Wallowa zone, appear to merge northward into a tectonically complicated corner ("upward arch") in the Juan de Fuca plate boundary [e.g., Weaver and Baker, 1988] which may play a role in accommodating shear along this zone.

Other crustal fault zones outside Oregon and Washington may contribute significant motion to the strain budget across the plate boundaries. These include primarily normal-oblique faulting along the Lewis and Clark zone, the Centennial zone, and faults north of the Wasatch zone [e.g., Stickney and Bartholomew, 1987; Anders et al., 1989; Smith and Sbar, 1974]. It is not clear whether motion across faults that form the northeastern boundary of the Basin and Range is included in the VLBI analysis for HATC and QUIN. The VLBI studies [e.g., Sauber, 1990; Argus and Gordon, 1991] use different inversion techniques and reference stations, and the relationship between the reference stations and fault activity in the northern Basin and Range is generally not addressed. If the Cascade graben and the Central Oregon fault zones, which form essentially long, narrow pull-apart basins, accommodate mostly transtensional strain as dextral shear takes the long en echelon right step from the eastern California-Walker Lane system to the western Washington-Vancouver Island-Queen Charlotte system, then the northern zones play a minor role. However, if motion along the eastern California-Walker Lane system dies out in a northward direction while the Olympic-Wallowa, Lewis and Clark, and other zones pick up the excess, then motion across these northeastern zones is important.

The young fault activity in Oregon and vicinity appears to join with the Eastern California shear zone [e.g., Dokka and Travis, 1990] and together form a much longer and broader "eastern shear zone" (Figure 1). Evidence for dextral shear that began in Miocene time is found locally along the entire zone. Distributed shear has played a major role in the rotation of crustal blocks [e.g., Wells and Heller, 1988; Wells, 1990] and in influencing the chemical composition, extrusion rates, and location of magmatism in the Pacific Northwest [e.g., Armstrong, 1978; Guffanti and Weaver, 1988; Sherrod and Smith, 1989]. The similarity in age and style of deformation supports a throughgoing zone that links Pacific-North American transform motion in coastal California with similar motion off southwestern Canada.

For many years investigators have called upon the oblique component of Juan de Fuca-North American plate convergence to drive right-lateral shear on faults in the Pacific Northwest. Indeed, arc-parallel strike-slip faulting is a common feature of obliquely convergent subduction zones around the world [e.g., Fitch, 1972; Jarrard, 1986]. However, late Quaternary fault activity around the northern margin of the Basin and Range appears to span a much larger region than is typically associated with oblique subduction and forms a classic rhombohedron (Figure 1). Although the pattern of

faulting in the Pacific Northwest may result from oblique subduction, recent motion of the Juan de Fuca plate system has been characterized by a general slowing and fragmentation that has been interpreted to indicate an unstable and passive Juan de Fuca plate under the influence of Pacific-North American plate motions [Crosson, 1972; Riddihough, 1984]. Deformation in the eastern zone continues or possibly accelerates during this time. As the Mendocino and Queen Charlotte triple junctions migrate closer together, the Juan de Fuca plate slows down, the length of the Cascade arc shrinks, and the eastern shear zone evolves toward more of a transform boundary. The Eastern California shear zone may have developed initially in a setting similar to that in central Oregon today, growing into a throughgoing zone as the Mendocino triple junction migrates northward [e.g., Weldon et al., 1993].

Right-lateral and extensional fault zones that cross Oregon and Washington may account for as much as 20% of the total Pacific-North American relative plate motion. The tectonic role of faults in the Pacific Northwest and those that form the northern boundary of the Basin and Range Province is important to the overall strain budget of Pacific-North American plate motion. More paleostrain information is needed to understand better the tectonic role of the eastern shear zone.

Acknowledgments. Most of this work was funded by a U. S. Geological Survey, National Earthquake Hazards Reduction Program grant (1434-92-G2193), a National Science Foundation Presidential Young Investigators Award (EAR 9057014), and an Oregon Department of Geology and Mineral Industries grant to RJW. Fieldwork was partially funded by a Geological Society of America Student Research Grant and an Oregon Department of Geology and Mineral Industries grant to SKP. Sincere thanks go to the property owners in central Oregon for access; C. Rosenfeld for aerial flights and photography; and G. Sega, R. Menton, C. Ryan, J. Stimac, and especially S. L. Pezzopane for field and production assistance. We appreciate G. Craven, C. Goldfinger, C. Mitchell, and R. Palmer for comments on earlier versions of this manuscript, and especially R. Dokka, P. Hooper, and R. Wells for their critical and insightful reviews, which significantly improved the final version.

REFERENCES

Aki, K., and P. G. Richards, Quantitative seismology: Theory and methods, 932 pp., W. H. Freeman, San Francisco, California, 1980.

Allison, I. S., Pluvial Fort Rock Lake, Lake County, Oregon, Oregon Dep. Geol. Min. Ind. Spec. Pap. 7, 72 pp., 1979.

Allison, I. S., Geology of Pluvial Lake Chewaucan Lake County, Oregon, 79 pp., Oregon State University Press, Corvallis, 1982.

Anders, M. H., J. W. Geissman, L. A. Piety, and J. T. Sullivan, Parabolic distribution of circumeastern Snake River Plain seismicity and Latest Quaternary faulting: Migratory pattern and association with the Yellowstone hotspot, J. Geophys. Res., 94, 1589-1621, 1989.

Appelgate B., C. Goldfinger, M. E. MacKay, L. D. Kulm, C. G. Fox, R. W. Embley, and P. J. Meis, A left-lateral strike-slip fault seaward of the Oregon convergent margin, Tectonics, 11, 465-477 1992.

Argus, D. F., and R. G. Gordon, Current Sierra Nevada-North America motion from very long baseline interferometry: Implications for the kinematics of the western United States, Geology, 19, 1085-1088, 1991.

Atwater, T., Implication of plate tectonics for Cenozoic tectonic evolution for Western North America, Geol. Soc. Am. Bull., 81, 3513-3536, 1970.

Aydin, A., and R. A. Schultz, Effect of mechanical interaction on the development of strike-slip faults with echelon patterns, J. Struct. Geol., 12, 123-129, 1990.

Bacon, C. R., Implications of silicic vent patterns for the presence of large crustal magma chambers, J. Geophys. Res., 90, 11,243-11,252, 1985.

Balster, C. A., and R. B. Parsons, Geomorphology and soils, Willamette Valley, Oregon, Agric. Exp. St. Special Rep. 265, 17 pp., Oregon State Univ., Corvallis, 1968.

Barker, J. S., and C. A. Langston, A teleseismic body-wave analysis of the May 1980 Mammoth Lakes, California, earthquakes, Bull. Seismol. Soc. Am., 73, 419-434, 1983.

Barker, J. S., and T. C. Wallace, A note on the teleseismic body waves from the 23 November 1984 Round Valley, California, earthquake, Bull. Seismol. Soc. Am., 76, 883-888, 1986.

Beeson, M. H., and T. L. Tolan, The Columbia River basalt group in the Cascade Range: A middle Miocene reference datum for structural analysis, J. Geophys. Res., 95, 19,547-19,559, 1990.

Beeson, M. H., T. L. Tolan, and J. L. Anderson, The Columbia River Basalt Group in western Oregon; Geologic structures and other factors that controlled flow emplacement patterns, in Volcanism and Tectonism in the Columbia River Flood-Basalt Province, Geol. Soc. Am. Spec. Pap. 239, edited by S. P. Reidel, and P. R. Hooper, pp. 223-246, 1989.

Bell, E. J., Overview of Late Cenozoic tectonics of the Walker Lane, in Western Geological Excursions, Annual Meetings of the Geological Society America and Affiliated Societies at Reno, Nevada, edited by Lintz, J. Jr., pp. 407-413, 1984.

Bell, E. J., and D. B. Slemmons, Neotectonic analysis of the northern Walker Lane, western Nevada and northern California (abstract), Geol. Soc. Am. Abstr. Programs, 14, 148, 1982a.

Bell, E. J., and D. B. Slemmons, Tectonic activity in the Smoke Creek Desert, northwestern Nevada (abstract), Geol. Soc. Am. Abstr. Programs, 14, 148-149, 1982b.

Benson, L. V., and R. S. Thompson, Lake-level variation in the Lahontan Basin for the past 50,000 years, Quat. Res., 28, 69-85, 1987.

Bond, J. G., and C. H. Wood, Geologic Map of Idaho, scale 1:500,000, Idaho Dep. of Lands, Bur. of Mines and Geol., Moscow, Idaho, 1978.

Bonilla, M. G., R. F. Mark, and J. J. Lienkaemper, Statistical relations among earthquake magnitude, surface rupture length, and surface fault displacement, Bull. Seismol. Soc. Am., 74, 2379-2411, 1984.

Brown, D. E., N. V. Peterson, G. D. McLean, Preliminary geology and geothermal resource potential of the Lakeview Area, Oregon, Oregon Dep. Geol. Min. Ind. Open File Rep. 0-80-9, 52 pp., Portland, Oregon, 1980.

Brune, J. N., Seismic movement, seismicity, and rate of slip along major fault zones, J. Geophys. Res., 73, 777-784, 1968.

Burchfiel, B. C., K. V. Hodges, and L. H. Royden, Geology of the Panamint Valley-Saline Valley pull apart system, California, J. Geophys. Res., 92, 10,422-10,426, 1987.

Campbell, N. P., and R. D. Bentley, Late Quaternary deformation of the Toppenish Ridge uplift in south-central Washington, Geology, 9, 519-524, 1981.

Chorowicz, J., and C. Sorlien, Oblique extensional tectonics in the Malawi Rift, Africa, Geol. Soc. Am. Bull., 104, 1015-1023, 1992.

Clark, T. A., D. Gordon, W. E. Himwich, C. Ma, A. Mallama, and J. W. Ryan, Determination of relative site motions in the Western United States using mark III very long baseline interferometry, J. Geophys. Res., 92, 12,741-12,750, 1987.

Cockerham, R. S., and E. J. Corbett, The July 1986 Chalfant Valley, California, earthquake sequence: Preliminary results, Bull. Seismol. Soc. Am., 77, 280-289, 1987.

Couch, R. W., and R. P. Lowell, Earthquakes and seismic energy release in Oregon, Ore Bin, 33, 61-84, 1971.

Craven, G. F., The tectonic development and late Quaternary deformation of Warner Valley south of Hart Mountain, Oregon, M.S. thesis, 94 pp., Humboldt State Univ. of California, Arcata, Oct. 1991.

Crosson, R. S., Small earthquakes, structure, and tectonics of the Puget Sound region, Bull. Seismol. Soc. Am., 62, 1133-1171, 1972.

Crosson, R. S., and D. Frank, The Mount Rainier earthquake of July 18, 1973, and its tectonic significance, Bull. Seismol. Soc. Am., 65, 393-401, 1975.

DeMets, C., R. G. Gordon, S. Stein, and D. F. Argus, A revised estimate of Pacific-North America motion and implications for Western North America plate boundary zone tectonics, Geophys. Res. Lett., 14, 911-914, 1987.

DeMets, C, R. G. Gordon, D. F. Argus, and S. Stein, Current plate motions, Geophys. J. Int., 101, 425-478, 1990.

dePolo, C. M., D. G. Clark, D. B. Slemmons, and A. R. Ramelli, Historical surface faulting in the Basin and Range Province, western North America: Implications for fault segmentation, J. Struct. Geol., 13, 123-136, 1991.

Dibblee, T. W., Jr., Areal geology of the western Mojave Desert, California, U. S. Geol. Surv. Prof. Pap. 522, 153 pp., 1967.

Dodge, R. L., and L. T. Grose, Tectonic and geomorphic evolution of the Black Rock Fault, northwestern Nevada, in, Earthquake Hazards Along the Wasatch Sierra-Nevada Frontal Fault Zones, U. S. Geol. Surv. Open File Rep. 80-801, edited by E. Anderson, A. Ryall, R. S. Smith, J. F. Evernden, J. F. Andriese, pp. 494-508, 1979.

Dokka, R. K., Displacements on late Cenozoic strike-slip faults of the central Mojave Desert, California, Geology, 11, 305-308, 1983.

Dokka, R. K., and C. J. Travis, Late Cenozoic strike-slip faulting in the Mojave Desert, California, Tectonics, 9, 311-340, 1990.

Donath, R., Analysis of basin-range structure, south-central Oregon, Geol. Soc. Am. Bull., 73, 1-16, 1962.

Donnelly-Nolan, J. M., D. E. Champion, C. D. Miller, T. L. Grove, and D. A. Trimble, Post-11,000-year volcanism at Medicine Lake Volcano, Cascade Range, Northern California, J. Geophys. Res., 95, 19,693-19,704, 1990.

Doser, D. I., Earthquake processes in the Rainbow Mountain-Fairview Peak-Dixie Valley, Nevada, region 1954-1959, J. Geophys. Res., 91, 12,572-12,586, 1986.

Doser, D. I., Modeling the Pnl waveforms of the Fairview Peak-Dixie Valley, Nevada, U.S.A. earthquake sequence (1954-1959), Phys. Earth Planet. Inter., 48, 64-72, 1987.

Doser, D. I., Source parameters of earthquakes in the Nevada Seismic Zone, 1915-1943, J. Geophys. Res., 93, 15,001-15,015, 1988.

Doser, D. I, The Character of Faulting Processes of Earthquakes in the Intermountain Region, in Fault Segmentation and Controls of Rupture Initiation and Termination, U. S. Geol. Surv. Open File Rep. 89-315, edited by D. P. Schwartz, and R. H. Sibson, pp. 163-180, 1989.

Eddington, P. K., R. B. Smith, and C. Renggli, Kinematics of Basin and Range intraplate extension, in Continental Extensional Tectonics, Geol. Soc. Am. Spec. Pub. 28, edited by M. P. Coward, J. F. Dewey, and P. L. Hancock, pp. 371-392, 1987.

Ekstrom, G., and P. England, Seismic strain rates in regions of distributed continental deformation, J. Geophys. Res., 94, 10,231-10,257, 1989.

England, P., and R. E. Wells, Neogene rotations and quasicontinuous deformation of the Pacific Northwest continental margin, Geology, 19, 978-981, 1991.

Fitch, T. J., Plate convergence, transcurrent faults, and internal deformation adjacent to Southeast Asia and the Western Pacific, J. Geophys. Res., 77, 4432-4460, 1972.

Fournier, R. O., Maximum depths of earthquakes as an aid in evaluating convective and conductive heat fluxes from the Cascade province and adjacent regions, in Geological, Geophysical, and Tectonic Setting of the Cascade Range, U. S. Geol. Surv. Open File Rep. 89-178, edited by L. J. Muffler, C. S. Weaver, and D. D. Blackwell, pp. 171-198, 1989.

Freidel, D. E., and P. F. McDowell, Late-Quaternary paleolakes in the Fort Rock Basin, Alkali, and Chewaucan Basins, in Active Faulting in South-central Oregon, Guidebook to Geol. Soc. Am. Fieldtrip #5, Cordilleran Meeting, Eugene, Oregon, 1992.

Gehrels, G. E., R. White, and G. Davis, La Grande pull apart basin (abstract), Geol. Soc. Am. Abstr. Programs., 12, 107, 1980.

Goldfinger, C., L. D. Kulm, R. S. Yeats, B. Appelgate, M. E. MacKay, and G. F. Moore, Transverse structural trends along the Oregon convergent margin: Implications for Cascadia earthquake potential and crustal rotations, Geology, 20, 141-144, 1992a.

Goldfinger, C., L. D. Kulm, R. S. Yeats, C. Mitchell, R. Weldon, II, C. Peterson, M. Darienzo, W. Grant, and G. R. Priest, Neotectonic map of the Oregon continental margin and adjacent abyssal plain, Oregon Dep. Geol. Min. Ind. Open File Rep. 0-92-4, 1992b.

Goles, G. G., and R. ST. J. Lambert, A strontium isotopic study of Newberry volcano, central Oregon: Structural and thermal implications, J. Volcanol. Geotherm. Res., 43, 159-174, 1990.

Grose, T. L. T., G. J. Saucedo, and D. L. Wagner, The Walker Lane in northeastern California (abstract), Eos Trans. AGU, 70, 1362, 1989.

Guffanti, M., and C. S. Weaver, Distribution of late Cenozoic volcanic vents in the Cascade Range: Volcanic arc segmentation and regional tectonic considerations, J. Geophys. Res., 93, 6513-6529, 1988.

Guffanti, M., M. A. Clynne, J. G. Smith, L. J. P. Muffler, and T. D. Bullen, Late Cenozoic volcanism, subduction, and extension in the Lassen Region of California, southern Cascade Range, J. Geophys. Res., 95, 19,453-19,464, 1990.

Gutmanis, J. C., Wrench faults, pull-apart basins, and volcanism in central Oregon: A new tectonic model based on image interpretation, Geology, 24, 183-192, 1989.

Haines, A. J., Calculating velocity fields across plate boundaries from observed shear rates, Geophys. J. R. Astron. Soc., 68, 203, 1982.

Hamilton, W., and W. B. Myers, Cenozoic tectonics of the Western United States, Rev. Geophys., 4, 509-536, 1966.

Hammond, P. E., J. L. Anderson, and K., J. Manning, Guide to the geology of the upper Clackamas and North Santiam Rivers area, northern Oregon Cascade Range, in Geologic field trips in Western Oregon and Southwestern Washington: Oregon Dep. Geol. Min. Ind. Bull. 101, 133-167, 1980.

Hanks, T. C., and H. Kanamori, A moment-magnitude scale, J. Geophys. Res., 84, 2348-2350, 1979.

Hedel, C. W., Late Quaternary faulting in Western Surprise Valley, Modoc County, California, M.S. thesis, 113 pp., San Jose State Univ. of California, Aug. 1980.

Hedel, C. W., Map showing geomorphic and geologic evidence for late Quaternary displacement along the Surprise Valley and associated faults, Modoc County, California, scale 1:62,500, Misc. Field Stud. Map MF-1429, 2 sheets, U. S. Geol. Survey, Menlo Park, Calif., 1984.

Hemphill-Haley, M. A., Quaternary stratigraphy and late Holocene faulting along the base of the eastern escarpment of Steens Mountain, southeastern Oregon, M.A. thesis, 87 pp., Humboldt State Univ., Arcata, Calif., 1987.

Hemphill-Haley, M. A., W. D. Page, R. Burke, and G. A. Carver, Holocene activity of the Alvord Fault, Steens Mountain, southeastern Oregon (report), 38 pp., Woodward-Clyde Consultants, Oakland, Calif., 1989.

Herd, D. G., Intracontinental plate boundary east of Cape Mendocino, California, Geology, 6, 721-725, 1978.

Hooper, P. R., and R. M. Conrey, A model for the tectonic setting of the Columbia River basalt eruptions, in Volcanism and Tectonism in the Columbia River Flood-Basalt Province, Geol. Soc. Am. Spec. Pap. 239, edited by S. P. Reidel, and P. R. Hooper, pp. 293-306, 1989.

Humphreys, E. D., and R. J. Weldon, Kinematic constraints on the rifting of Baja California, in The Gulf and Peninsular Provinces of the Californias: Mem. Am. Assoc. Pet. Geol., 47, edited by J. P. Dauphin, and B. R. T. Simoneit, 217-229, 1991.

Jackson, J., and D. McKenzie, The relationship between plate motions and seismic moment tensors, and the rates of active deformation in the Mediterranean and Middle East, Geophys. J., 93, 45-73, 1988.

Jarrard, R. D., Relations among subduction parameters, Rev. Geophy., 24, 217-284, 1986.

Jennings, C. W., Preliminary fault activity map of California, scale 1:750,000, Calif. Div. of Mines and Geol., Sacramento, 1992.

Kanamori, H., Magnitude scale and quantification of earthquakes, Tectonophysics, 93, 185-199, 1983.

Kelsey, H. M., and G. A. Carver, Late Neogene and Quaternary tectonics associated with northward growth of the San Andreas Transform Fault, northern California, J. Geophys. Res., 93, 4797-4819, 1988.

Kelsey, H., C. E. Mitchell, R. J. Weldon, D. Engebretson, R. Ticknor, and J. Bockheim, Latitudinal variation in surface uplift from geodetic, wavecut platform and topographic data, Cascadia Margin (abstract), Geol. Soc. Am. Abstr. Programs, 24, 37, 1992.

Klein, F. W., Earthquakes in Lassen Volcanic National Park, California, Bull. Seismol. Soc. Am., 69, 867-975, 1979.

Kostrov, V. V., Seismic moment and energy of earthquakes, and seismic flow of rock, Izv. Acad. Sci. USSR Phys. Solid Earth, Engl. Transl., 1, 23-44, 1974.

Lawrence, R. D., Strike-slip faulting terminates the Basin and Range province in Oregon, Geol. Soc. Am. Bull., 87, 846-850, 1976.

Lindberg, D. N., Extending the zone of recognized late-Holocene faulting in the Basin and Range of southeastern Oregon (abstract), Geol. Soc. Am. Abstr. Programs, 21, 106, 1989.

Lubetkin, L. K. C., and M. M. Clark, Late Quaternary activity along the Lone Pine fault, eastern California, Geol. Soc. Am. Bull., 100, 755-766, 1988.

Ludwin, R. S., C. S. Weaver, and R. S. Crosson, Seismicity of Washington and Oregon, in Neotectonics of North America, vol. 1, Decade Map edited by D. B. Slemmons, E. R. Engdahl, M. D. Zoback, and D. D. Blackwell, pp. 77-98, Geological Society of America, Boulder, Colo., 1991.

MacLeod, N. S., and D. R. Sherrod, Geologic evidence for a magma chamber beneath Newberry volcano, Oregon, J. Geophys. Res., 93, 10,067-10,079, 1988.

Magill, J. R., R. E. Wells, R. W. Simpson, and A. V. Cox, Post 12 m.y. rotation of southwest Washington, J. Geophys. Res., 87, 3761-3776, 1982.

Mann, G. M., Seismicity and Late Cenozoic faulting in the Brownlee Dam area--Oregon - Idaho: A preliminary report, U. S. Geol. Surv. Open File Rep. 89-429, 46 pp., 1989.

Mann, G. M. and C. E. Meyer, Late Cenozoic structure and correlations to seismicity along the Olympic-Wallowa lineament, Geol. Soc. of Am. Bull., in press, 1993.

McInelly, G. W., and H. M. Kelsey, Later Quaternary, tectonic deformation in the Cape Arago-Bandon region of coastal Oregon as deduced from wave-cut platforms, J. Geophys. Res., 95, 6699-6713, 1990.

Minster, J. B., and T. H. Jordan, Present-day plate motions, J. Geophys. Res., 83, 5331-5351, 1978.

Minster, J. B., and T. H. Jordan, Vector constraints on Quaternary deformation of the western United States east and west of the San Andreas fault, in Tectonics and Sedimentation along the California margin: Pacific Section, 38, edited by J. K. Crouch, and S. B. Bachman, pp. 1-16, Society for Economic Paleontologists and Mineralogists, Tulsa, Okla., 1984.

Minster, J. B., and T. H. Jordan, Vector constraints on western U. S. deformation from space geodesy, neotectonics, and plate motions, J. Geophys. Res., 92, 2798-4804, 1987.

Molnar, P., Average regional strain due to slip on numerous faults of different orientations, J. Geophys. Res., 88, 6430-6432, 1983.

Molnar, P., and Q. Deng, Faulting associated with large earthquakes and the average rate of deformation in central and eastern Asia, J. Geophys. Res., 89, 6203, 1984.

Moore, G. W., (Ed.), Plate-Tectonic Map of the Circum-Pacific Region, published by the Circum-Pacific Council for Energy and Min. Resour., Washington D.C., 1982.

Muffler, L. J. P., and M. A. Clynne, Late Quaternary faulting of the Hat Creek basalt (abstract), Eos Trans. AGU, 70, 1310, 1989.

Nakata, J. K., C. M. Wentworth, and M. Machette, Quaternary fault map of the Basin and Range and Rio Grande Rift Provinces, western United States, U. S. Geol. Surv. Open File Rep., 82-579, 1982.

Nakata, T, R. J. Weldon, S. K. Pezzopane, C. Rosenfeld, and R. S. Yeats, Preliminary aerial photo-interpretation of active faults in Oregon (abstract), Geol. Soc. Am. Abstr. Programs, 24, 72, 1992.

Negrini, R. M., and J. O. Davis, Dating late Pleistocene pluvial events and tephras by correlating paleomagnetic secular variation records from the Western Great Basin, Quat. Res., 37, 1992.

Nishimura, C., D. S. Wilson, and R. N. Hey, Pole of rotation analysis of present-day Juan De Fuca plate motion, J. Geophys. Res., 89, 10,283-10,290, 1984.

Noson, L. L., A. Qamar, and G. W. Thorsen, Washington state earthquake hazards, Inf. Circ. 85, 75 pp., Washington Div. of Geol. and Earth Resour., 1988.

Patton, H. J., P-wave fault-plane solutions and the generation of surface waves by earthquakes in the western United States, Geophys. Res. Lett., 12, 518-521, 1985.

Patton, H. J., and G. Zandt, Seismic moment tensors of Western U. S. earthquakes and implications for the tectonic stress field, J. Geophys. Res., 96, 18,245-18,259, 1991.

Pease, R. W., Normal faulting and lateral shear in northeastern California, Geol. Soc. Am. Bull., 80, 715-720, 1969.

Peterson, N. V., and E. A., Groh, Crack-in-the-ground, Lake County, Oregon, Ore Bin, 26, 158-166, 1964.

Pezzopane S. K., Active faults and earthquake ground motions in Oregon, Ph. D. dissertation, 208 pp., University of Oregon, Eugene, March 1993.

Pezzopane, S. K., and R. J. Weldon, Holocene fault activity between the Basin and Range and High

Cascades, Oregon (abstract), Eos Trans. AGU, 71, 1608, 1990.
Pezzopane S. K., T. Nakata, and R. J. Weldon, Preliminary active fault map for Oregon (abstract), Geol. Soc. Am. Abstr. Programs, 24, 74, 1992.
Powell, R. E., Geology of the crystalline basement complex, eastern Transverse Ranges, southern California: Constraints on regional tectonic interpretations, Ph.D. dissertation, 441 pp., California Institute of Technology, Pasadena, Calif., 1981.
Powell, R. E., Balanced palinspastic reconstruction of pre-late Cenozoic paleogeology, southern California: Constraints on kinematic evolution of the San Andreas fault system, in The San Andreas Fault System: Displacement, Palinspastic Reconstruction, and Geologic Evolution, Geol. Soc. Am. Mem. 178, 1-106, edited by R. E. Powell, R. J. Weldon, and J. C. Matti, 1993.
Powell, R. E., and R. J. Weldon, Evolution of the San Andreas fault, Annu. Rev. Earth Planet. Sci. 20, 431-468, 1992.
Priest, G. R., N. M. Woller, G. L. Black, and S. H. Evans, Geology and geothermal resources of the central Oregon Cascade Range, Oregon Dep. Geol. Min. Ind. Spec. Pap. 15, edited by G. R. Priest, and B. F. Vogt, 96 pp., 1983.
Raisz, E., The Olympic-Wallowa Lineament, Am. J. Sci., 243-A, 479-485, 1945.
Rasmussen, J., and E. Humphreys, Tomographic image of the Juan de Fuca plate beneath Washington and western Oregon using teleseismic P-wave travel times, Geophys. Res. Lett., 15, 1417-1420, 1988.
Reches, Z., Faulting of rocks in three-dimensional strain fields, II. Theoretical analysis, Tectonophysics, 95, 133-156, 1983.
Reidel, S. P., The Saddle Mountains: The evolution of an anticline in the Yakima fold belt, Am. J. Sci., 284, 942-978, 1984.
Richard, S. M., (Ed.), Deformation associated with the Neogene Eastern California Shear Zone, southeastern California and southwestern Arizona, in Proceedings of the workshop on the Eastern California Shear Zone, 78 pp., San Bernardino County Museums Spec. Pub. 92-1, Redlands, California, 1992.
Riddihough, R., Recent movements of the Juan de Fuca plate system, J. Geophys. Res., 89, 6980-6994, 1984.
Ring, U., C. Betzler, and D. Delvaux, Normal vs. strike-slip faulting during rift development in East Africa: The Malawi rift, Geology, 20, 1015-1018, 1992.
Roberts, C. T., and T. L. T. Grose, Late Cenozoic extension strain rates and directions in the Honey Lake-Eagle Lake region, northeastern California (abstract), Eos Trans. AGU, 63, 1982.
Rogers, G. C., Earthquake fault plane solutions near Vancouver Island, Can. J. Earth Sci., 16, 523-531, 1979.
Russell, I. C., A geological reconnaissance in southern Oregon, U. S. Geol. Surv. Ann. Rep., 4, 431-464, 1884.
Sauber, J., Geodetic measurement of deformation in California, NASA Tech. Mem. 100732, 211 pp., 1990.
Sauber, J., W. Thatcher, and S. Solomon, Geodetic measurements of deformation in the central Mojave Desert, California, J. Geophys. Res., 91, 12,683-12,693, 1986.
Savage, J. C., and M. Lisowski, Strain measurements and potential for a great subduction earthquake off Oregon and Washington, Science, 252, 101-103, 1991.
Savage, J. C., M. Lisowski, and W. H. Prescott, An apparent shear zone trending north-northwest across the Mojave Desert into Owens Valley, eastern California, Geophys. Res. Lett., 17, 2113-2116, 1990.
Savage, J. C., M. Lisowski, and W. H. Prescott, Strain accumulation in western Washington, J. Geophys. Res., 96, 14,493-14,507, 1991.
Schaff, S., The 1968 Adel, Oregon, earthquake swarm, M.S. thesis, Univ. of Nevada at Reno, 1976.
Scholz, C. H., Scaling laws for large earthquakes: Consequences for physical models, Bull. Seismol. Soc. Am., 72, 1-14, 1982.
Scholz, C. H., and P. A. Cowie, Determination of total strain from faulting using slip measurements, Nature, 346, 837-839, 1990.
Shawe, D. R., Strike-slip control of Basin-Range structure indicated by historical faults in western Nevada, Geol. Soc. Am. Bull., 76, 1361-1378, 1965.
Sherrod, D. R., and L. G. Pickthorn, Some notes on the Neogene structural evolution of the Cascade Range in Oregon, in Geological, Geophysical, and Tectonic Setting of the Cascade Range, U. S. Geol. Surv. Open File Rep. 89-178, edited by L. J. P. Muffler, C. S. Weaver, and D. D. Blackwell, pp. 351-368, 1989.
Sherrod, D. R., and J. G. Smith, Quaternary extrusion rates from the Cascade Range, northwestern United States and British Columbia, in Geological, Geophysical, and Tectonic Setting of the Cascade Range, U. S. Geol. Surv. Open File Rep. 89-178, edited by L. J. P. Muffler, C. S. Weaver, and D. D. Blackwell, pp. 94-103, 1989.
Sibson, R. H., Fault zone models, heat flow, and the depth distribution of earthquakes in continental crust of the United States, Bull. Seismol. Soc. Am., 72, 151-163, 1982.
Simpson, G. D., Late Quaternary tectonic development of the northwestern part of the Summer Lake basin, south-central Oregon, M.S. thesis, Humboldt State Univ. of Calif., Arcata, May 1990.
Smith, G. I., and F. A. Street-Perrott, Pluvial lakes of the western United States, in Late Quaternary Environment of the United States, vol. 1, The late Pleistocene, edited by S. C. Porter and H. E. Wright, pp. 190-212, University of Minnesota Press, Minneapolis, 1983.
Smith, R. B., Seismicity, crustal structure, and intraplate tectonics of the interior of the western Cordillera, in Cenozoic Tectonics and Regional Geophysics of the Western Cordillera, Geol. Soc. Am. Mem. 152, edited by R. B. Smith, G. P. Eaton, pp. 111-114, 1978.
Smith, R. B., and A. G. Lindh, Fault-plane solutions of the western United States: A compilation, in Cenozoic Tectonics and Regional Geophysics of the Western Cordillera, Geol. Soc. Am. Mem. 152, edited by R. B. Smith, G. P. Eaton, pp. 107-109, 1978.
Smith, R. B., and M. L. Sbar, Contemporary tectonics and seismicity of the Western United States with emphasis on the Intermountain seismic belt, Geol. Soc. Am. Bull., 85, 1205-1218, 1974.
Spence, W., Stress Origins and Earthquake Potentials in Cascadia, J. Geophys. Res., 94, 3076-3088, 1989.
Stewart, J. H., and J. E. Carlson, Geologic Map of Nevada, scale 1:500,000, U. S. Geol. Surv. and Nev. Bur. of Mines and Geol., 1978.
Stewart, J. H., J. P. Albers, and F. G. Poole, Summary of regional evidence for right-lateral displacement in the western Great Basin, Geol. Soc. Am. Bull., 79, 1407-1414, 1968.
Stewart, J. H., G. W. Walker, and F. J. Kleinhampl, Oregon-Nevada lineament, Geology, 3, 265-268, 1975.
Stickney, M. C., and M. J. Bartholomew, Seismicity and late quaternary faulting of the Northern Basin and Range Province, Montana and Idaho, Bull. Seismol. Soc. Am., 77, 1602-1625, 1987.
Stimac, J., and R. J. Weldon, Paleomagnetism and tectonic rotations of the Rattlesnake and Devine Canyon ash-flow tuffs, northern Basin and Range, southern Oregon (abstract), Geol. Soc. Am. Abstr. Programs, 24, 83, 1992.
Taylor, E. M., Volcanic history and tectonic development of the Central High Cascade Range, Oregon, J. Geophys. Res., 95, 19,611-19,622, 1990.
Thatcher, W., and T. Hanks, Source parameters of southern California earthquakes, J. Geophys. Res., 78, 8547-8576, 1973.
Tolan, T. L., and S. P. Reidel, Structure map of a portion of the Columbia River flood-basalt Province, in Volcanism and Tectonism in the Columbia River Flood-Basalt Province, Geol. Soc. Am. Spec. Pap. 239, edited by S. P. Reidel, and P. R. Hooper, 386 pp., 1989.
U.S. Army Corps of Engineers, Portland District, Fern Ridge, Cottage Grove and Dorena Lakes earthquake and fault study, Design Mem., 9, 108 pp., 1981a.
U.S. Army Corps of Engineers, Portland District, Lookout Point, Dexter, Hills Creek and Fall Creek Lakes earthquake and fault study, Design Mem., 6, 100 pp., 1981b.
U.S. Army Corps of Engineers, Portland District, Cougar and Blue Lakes earthquake and fault study, Design Mem., 19, 90 pp., 1983a.
U.S. Army Corps of Engineers, Portland District, The Dalles and John Day Lakes earthquake and fault study, Design Mem., 26, 66 pp., 1983b.
Vink, G. E., W. J. Morgan, and W. L. Zhao, Preferential rifting of continents: A source of displaced terranes, J. Geophys. Res., 89, 10,072-10,076, 1984.
Wagner, D. L., G. J. Saucedo, and T. L. T. Grose, The Honey Lake fault zone, northeastern California, its nature, age, and displacement (abstract), Eos Trans. AGU, 70, 1358, 1989.
Waitt, R. B., Late Cenozoic deposits, landforms, stratigraphy, and tectonism in Kittitas Valley, Washington, U. S. Geol. Surv. Prof. Pap. 1127, 18 pp., 1979.
Walker, G. W., Geologic map of Oregon east of the 121st meridian, scale 1:500,000, U. S. Geol. Surv. Map I-902, 1977.
Walker G W., and N. S. MacLeod, Geologic map of Oregon, 2 sheets, scale 1:500,000, U. S. Geol. Survey, Washington, D. C., 1991.
Walker, G. W., N. V. Peterson, and R. C. Greene, Reconnaissance geologic map of the east half of the Crescent quadrangle, Lake, Deschutes, and Crook counties, Oregon, scale 1:250,000, U. S. Geol. Surv. Map I-493, 1967.
Wallace, R. E., Patterns and timing of Late Quaternary faulting in the Great Basin Province and relation to some regional tectonic features, J. Geophys. Res., 89, 5763-5769, 1984.
Wallace, T. C., D. V. Helmberger, and G. R. Mellman, A technique for the inversion of regional data in source parameter studies, J. Geophys. Res., 86, 1679-1685, 1981.
Walsh, T. J., Korosec, M. A., W. M. Phillips, R. L. Logan, and H. W. Schasse, Geologic map of Washington southwest quadrant, Geol. Map GM-34, Wash. Div.of Geol. and Earth Resour., Olympia, 1987.
Ward, S. N., Pacific-North America plate motions: New results from very long baseline interferometry, J. Geophys. Res., 95, 21,965-21,981, 1990.
Weaver, C. S., and G. E. Baker, Geometry of the Juan de Fuca Plate beneath Washington and northern Oregon from seismicity, Bull. Seismol. Soc. Am., 78, 264-275, 1988.
Weaver, C. S., W. C. Grant, and J. E. Shemeta, Local crustal extension at Mount St. Helens, Washington, J. Geophys. Res., 92, 10,170-10,178, 1987.
Weide, D. L., Postglacial geomorphology and environments of the Warner Valley - Hart Mountain area, Oregon, Ph.D. dissertation, University of California at Los Angeles, 1975.
Weldon, R., and E. Humphreys, A kinematic model of Southern California, Tectonics, 5, 33-48, 1986.
Weldon, R. J., K. E. Meisling, and J. Alexander, A speculative history of the San Andreas fault in the central Transverse Ranges, California, in The San Andreas Fault System; Displacement, Palinspastic Reconstruction, and Geologic Evolution: Boulder, Colorado, Geol. Soc. Am. Mem. 178, 161-189, edited by R. E. Powell, R. J. Weldon, and J. C. Matti, 1993.
Wells, R. E., Paleomagnetic rotations and the Cenozoic tectonics of the Cascade Arc, Washington, Oregon, and California, J. Geophys. Res., 95, 19,409-19,417, 1990.
Wells, R. E., and P. L. Heller, The relative contribution of accretion, shear, and extension to Cenozoic tectonic rotation in the Pacific Northwest, Geol. Soc. Am. Bull., 100, 325-338, 1988.
Werner, K., J. Nabelek, R. Yeats, and S. Malone, The Mount Angel fault: Implications of seismic-reflection data and the Woodburn, Oregon, Earthquake sequence of August 1990, Oregon Geol., 54, 112-117, 1992.
Wernicke, B., G. J. Axen, and J. K. Snow, Basin and Range extensional tectonics at the latitude of Las Vegas, Nevada, Geol. Soc. Am. Bull., 100, 1738-1757, 1988.
Wesnousky, S. G., C. H. Scholz, and K. Shimazaki, Deformation of an island arc: Rates of moment release and crustal shortening in intraplate Japan determined from seismicity and Quaternary fault data, J. Geophys. Res., 87, 6829-6852, 1982.

Wesnousky, S. G., L. M. Jones, C. H. Scholz, and Q. Deng, Historical seismicity and rates of crustal deformation along the margins of the Ordos Block, north China, Bull. Seismol. Soc. Am., 74, 1767-1783, 1984.

West, M. W., and M. E. Shaffer, Late Quaternary tectonic deformation in the Smyrna bench and saddle gap segments, Saddle Mountains anticline, Yakima fold belt, central Columbia Basin, Washington (abstract), Geol. Soc. Am. Abstr. Programs., 21, 157, 1989.

Wills, C. J., Active faults north of Lassen Volcanic National Park, northern California, California Geology, 44, 51-58, 1991.

Wills, C. J., and G. Borcherdt, Holocene slip rate and earthquake recurrence on the Honey Lake fault zone, northeastern California (abstract), Eos Trans. AGU, 71, 1608, 1990.

Wilson, J. R., M. J. Bartholomew, and R. J. Carson, Late Quaternary faults and their relationship to tectonism in the Olympic Peninsula, Washington, Geology, 7, 235-239, 1979.

Wise, D. U., An outrageous hypothesis for the tectonic pattern of the North American Cordillera, Geol. Soc. Am. Bull., 74, 357-362, 1963.

Withjack, M. O., and W. R. Jamison, Deformation produced by oblique rifting, Tectonophysics, 126, 99-124, 1986.

Wood, S. H., Evaluation of potential geologic hazards proposed Valbois Destination Resort, Valley County, West-central Idaho, report prepared for Valbois Inc., 35 pp., Oct., 1990.

Wright, L., Late Cenozoic fault patterns and stress fields in the Great Basin and westward displacement of the Sierra Nevada block, Geology, 4, 489-494, 1976.

Yeats, R. S., A search for active faults in the Willamette Valley, Oregon, in U.S. Geol. Sur. NEHRP Summaries of Tech. Rep., 30, pp. 530-536, 1990a.

Yeats, R. S., A search for active faults in the Willamette Valley, Oregon, in U.S. Geol. Sur. NEHRP Summaries of Tech. Rep., 31, pp. 468-475, 1990b.

Yelin, T. S., and H. J. Patton, Seismotectonics of the Portland, Oregon region, Bull. Seism. Soc. Am., 81, 109-130, 1991.

Yount, J. C., and M. L. Holmes, The Seattle fault: a possible Quaternary reverse fault beneath Seattle, Washington (abstract), Geol. Soc. Am. Abstr. Programs., 24, 93, 1992.

Zhang, P., M. Ellis, D. B. Slemmons, and F. Mao, Right-lateral displacements and the Holocene slip rate associated with prehistoric earthquakes along the southern Panamint Valley fault zone: Implications for southern Basin and Range tectonics and Coastal California deformation, J. Geophys. Res., 95, 4857-4872, 1990.

Zoback, M. L., and G. A. Thompson, Basin and Range rifting in northern Nevada: Clues from a mid-Miocene rift and its subsequent offsets, Geology, 6, 111-116, 1978.

Zoback, M. L., R. E. Anderson, and G. A. Thompson, Cainozoic evolution of the state of stress and style of tectonism of the Basin and Range province of the western United States, R. Soc. London Philos. Trans., Ser. A, A300, 407-434, 1981.

Zollweg, J. E., and R. S. Jacobson, A seismic zone on the Oregon-Idaho border: The Powder River earthquakes of 1984, Bull. Seismol. Soc. Am., 76, 985-999, 1986.

S. K. Pezzopane, U.S. Geological Survey, Box 25046 MS 425, Denver Federal Center, Denver, CO 80225.

R. J. Weldon II, Department of Geological Sciences, University of Oregon, Eugene, OR 97403.

(Received July 11, 1991;
revised December 7, 1992;
accepted December 17, 1992.)